J. Nonlinear Sci. Vol. 6: pp. 169–199 (1996)

Journal of
Nonlinear
Science

A Nonlinear Extensible 4-Node Shell Element Based on Continuum Theory and Assumed Strain Interpolations*

P. Betsch and E. Stein
Institut für Baumechanik und Numerische Mechanik, Universität Hannover, Germany

Received October 17, 1995
Communicated by Jerrold Marsden and Stephen Wiggins

This paper is dedicated to the memory of Juan C. Simo†

Summary. A quadrilateral continuum-based C^0 shell element is presented, which relies on extensible director kinematics and incorporates unmodified three-dimensional constitutive models. The shell element is developed from the nonlinear enhanced assumed strain (EAS) method advocated by Simo & Armero [1] and formulated in curvilinear coordinates. Here, the EAS-expansion of the material displacement gradient leads to the local interpretation of enhanced covariant base vectors that are superposed on the compatible covariant base vectors. Two expansions of the enhanced covariant base vectors are given: first an extension of the underlying single extensible shell kinematic and second an improvement of the membrane part of the bilinear element. Furthermore, two assumed strain modifications of the compatible covariant strains are introduced such that the element performs well even in the case of very thin shells.

1. Introduction

Many finite shell elements that have been developed in recent years are based on the common kinematic assumption of inextensibility in the thickness direction and the zero normal stress condition; see e.g. [2]–[6]. According to the inextensibility constraint, a rotation tensor is required in order to treat large rotations.

An alternative approach relies on an extensible director kinematic which offers a very attractive numerical formulation since rotational degrees of freedom can be avoided. Thus, the corresponding update procedure for the extensible director is based on simple vector addition. Since the work of Simo, Rifai & Fox [7] on an extensible 4-node shell

* In honour of Professor Juan Simo who had significant collaboration with our institute and contributed important insights to our research work.

† This paper was solicited by the editors to be part of a volume dedicated to the memory of Juan Simo.

element, several other extensible shell formulations have been published. The 8-node extensible shell element of Büchter & Ramm [8] and Büchter, Ramm & Roehl [9] incorporates an enhanced assumed strain (EAS) expansion of the covariant thickness component of the Green-Lagrangian strain tensor. This expansion allows for the implementation of full three-dimensional constitutive models without resorting to the plane stress assumption. The plane stress condition is imposed in a weak sense; see also Steinmann, Betsch & Stein [10]. Additionally, the membrane part of the 4-node extensible shell element of Betsch, Gruttmann & Stein [11] has been improved by means of an expansion of the enhanced Green-Lagrangian strain tensor. The extensible shell formulation of Sansour [12] relies on a higher order shell kinematic that leads to seven nodal degrees of freedom. The same kinematic assumption has been investigated by Kühhorn & Schoop [13] within the context of sandwich shells. An alternative extensible shell element formulation of Parisch [14] employs three nodes in the thickness direction. The advantages of a six-degrees-of-freedom director shell theory have also been pointed out by Schoop [15].

Analogous to the works [8], [9] and [11], the present 4-node shell element relies on an EAS-expansion in order to facilitate the use of three-dimensional constitutive laws without any shell-specific modifications. However, we enhance the material displacement gradient instead of the Green-Lagrangian strain tensor. This approach coincides with the nonlinear EAS-method advocated by Simo & Armero [1] where the material displacement gradient has been used in order to extend the linear EAS-method of Simo & Rifai [16] to the nonlinear theory.

We recast the nonlinear EAS-method of Simo & Armero in terms of curvilinear coordinates. Within the curvilinear description the EAS-expansion of the material displacement gradient leads to the local interpretation of enhanced covariant base vectors which are superposed on the compatible covariant base vectors. Two expansions of the enhanced covariant base vectors are presented which both extend the underlying single extensible shell kinematic and improve the membrane part of the bilinear element.

Furthermore, two assumed strain modifications of the compatible covariant strains are employed in order to eliminate parasitic strain effects of the compatible low-order C^0 interpolations. The assumed strain interpolation of Dvorkin and Bathe [17] is a very powerful tool to overcome the shear locking effect of the 4-node displacement model. This modification of the compatible covariant shear strains has been intensely investigated by Bathe and Dvorkin [18] Stander, Matzenmiller and Ramm [19] and Parisch [20] and works well even for initially distorted meshes.

Analogous to the shear locking effect of low order plate and shell elements, the bilinear interpolation of the *extensible* director field leads to parasitic transverse normal strains which lead to locking in bending dominated situations, especially in the case of very thin shells and coarse meshes. To overcome this locking effect Betsch & Stein [21] have proposed a simple assumed strain interpolation of the compatible transverse normal strains. It has been shown in [21] that the assumed strain interpolation makes the extensible shell formulation competitive to more elaborate formulations which rely on an orthogonal matrix for the description of finite rotations. Thus the pathological behavior of the simple extensible director interpolation which has also been reported by Simo, Rifai & Fox [7] is completely eliminated by means of the assumed strain method.

First, we give a comprehensive account of the nonlinear EAS-method advocated by Simo & Armero [1] in conjunction with a representation in terms of curvilinear

coordinates. After introducing a single extensible director kinematic we present two EAS-expansions of the enhanced covariant base vectors. Then we proceed with the compatible finite element approximation and discuss alternative interpolations of the extensible director field. Finally we present a modification of the compatible constant transverse normal strains based on the assumed strain method [22]. Several numerical examples are used to verify that our newly developed formulation is able to deal with thin-shell structures as well as with large strain problems.

2. Weak Form of the EAS Formulation

Let $\boldsymbol{X}(\theta^i)$ denote the position vector of a material point in the initial configuration $\mathcal{B}_0$ described by a general curvilinear set of coordinates θ^i. The corresponding placement in the actual configuration $\mathcal{B}$ follows from $\boldsymbol{x}(\theta^i) = \boldsymbol{X}(\theta^i) + \boldsymbol{u}(\theta^i)$, where $\boldsymbol{u}$ is the displacement vector. Following Simo & Armero [1], the weak form of the nonlinear enhanced assumed strain method can be written

$$G_{int} + G_{dyn} - G_{ext} = 0, \tag{1}$$

with the internal virtual work contribution

$$G_{int} = \int_{\mathcal{B}_0} \left\{ \mathrm{Grad}[\delta \boldsymbol{u}] : [2\boldsymbol{F}\partial_{\boldsymbol{C}} W] + \delta \tilde{\boldsymbol{H}} : [2\boldsymbol{F}\partial_{\boldsymbol{C}} W - \boldsymbol{P}] - \delta \boldsymbol{P} : \tilde{\boldsymbol{H}} \right\} dV. \tag{2}$$

Accordingly, the weak form contains three independent fields: the displacements $\boldsymbol{u}$, the nominal stress tensor $\boldsymbol{P}$ and the enhanced displacement gradient $\tilde{\boldsymbol{H}}$. W denotes the strain energy density function per unit initial volume and $\boldsymbol{C} = \boldsymbol{F}^T\boldsymbol{F}$. The total deformation gradient is defined by

$$\boldsymbol{F} = \mathrm{Grad}[\boldsymbol{x}] + \tilde{\boldsymbol{H}}. \tag{3}$$

Within a finite element the discontinuous expansion of $\tilde{\boldsymbol{H}}$ is intended to enhance the compatible deformation gradient $\mathrm{Grad}[\boldsymbol{x}]$ which results from the finite element approximation of $\boldsymbol{x}$ due to the pure displacement formulation. In (1) the virtual work of the inertial forces is denoted by

$$G_{dyn} = \int_{\mathcal{B}_0} \delta \boldsymbol{u} \cdot \ddot{\boldsymbol{x}} \rho_0 \, dV \tag{4}$$

and the virtual work of the external loads is represented by

$$G_{ext} = \int_{\mathcal{B}_0} \delta \boldsymbol{u} \cdot \boldsymbol{b} \, dV + \int_{\partial \mathcal{B}_{0t}} \delta \boldsymbol{u} \cdot \bar{\boldsymbol{t}} \, dA. \tag{5}$$

It has been shown by Simo & Armero [1] that the nominal stress field can be eliminated from the weak form when the expansion of the enhanced displacement gradient satisfies the condition

$$\int_{\mathcal{B}_0} \tilde{\boldsymbol{H}} \, dV = \boldsymbol{0}. \tag{6}$$

This condition ensures that at least constant states of stress can be reproduced by the finite element model. It represents an important stability requirement of the method as has been shown within the infinitesimal theory by Simo & Rifai [16] and Reddy & Simo [23].

Accordingly, a two field formulation in terms of displacements $\boldsymbol{u}$ and the enhanced displacement gradient $\tilde{\boldsymbol{H}}$ remains. The internal virtual work (2) may now be written in the form

$$G_{int} = \int_{\mathcal{B}_0} \left\{ \mathrm{Grad}[\delta \boldsymbol{u}]^T \boldsymbol{F} + \delta \tilde{\boldsymbol{H}}^T \boldsymbol{F} \right\} : \widehat{\boldsymbol{S}}\, dV = \int_{\mathcal{B}_0} \left\{ \mathrm{grad}[\delta \boldsymbol{u}] + \delta \tilde{\boldsymbol{h}} \right\} : \widehat{\boldsymbol{\tau}}\, dV, \tag{7}$$

where the expressions

$$\mathrm{Grad}[\delta \boldsymbol{u}] = \mathrm{grad}[\delta \boldsymbol{u}]\boldsymbol{F} \qquad \text{and} \qquad \delta \tilde{\boldsymbol{H}} = \delta \tilde{\boldsymbol{h}} \boldsymbol{F} \tag{8}$$

have been used. In order to alleviate the notation, in (7) the 'constitutive' Second Piola Kirchhoff stress tensor

$$\widehat{\boldsymbol{S}} = 2\partial_{\boldsymbol{C}} W(\boldsymbol{C}) = \hat{S}^{ij} \boldsymbol{G}_i \otimes \boldsymbol{G}_j \tag{9}$$

and the 'constitutive' Kirchhoff stress tensor

$$\widehat{\boldsymbol{\tau}} = 2\boldsymbol{F}\partial_{\boldsymbol{C}} W(\boldsymbol{C})\boldsymbol{F}^T = \hat{S}^{ij} \boldsymbol{g}_i \otimes \boldsymbol{g}_j \tag{10}$$

have been defined. Throughout this paper the usual summation convention is used, where Latin indices range from 1 to 3 and Greek indices range from 1 to 2. The covariant base vectors of the reference configuration $\mathcal{B}_0$

$$\boldsymbol{G}_i = \frac{\partial \boldsymbol{X}}{\partial \theta^i} = \boldsymbol{X}_{,i} \tag{11}$$

are directed tangentially along the curvilinear coordinates θ^i. The corresponding covariant base vectors $\boldsymbol{g}_i$ of the deformed configuration $\mathcal{B}$ can be obtained with the help of the deformation gradient via $\boldsymbol{g}_i = \boldsymbol{F}\boldsymbol{G}_i$. The additive decomposition of the total deformation gradient (3) directly leads to an additive decomposition of the deformed base vectors into compatible and enhanced parts:

$$\boxed{\boldsymbol{g}_i = \boldsymbol{x}_{,i} + \widetilde{\boldsymbol{g}}_i} \tag{12}$$

Hence, the compatible part of the deformation gradient

$$\mathrm{Grad}[\boldsymbol{x}] = \boldsymbol{x}_{,i} \otimes \boldsymbol{G}^i \tag{13}$$

is locally superposed by the enhanced displacement gradient

$$\tilde{\boldsymbol{H}} = \widetilde{\boldsymbol{g}}_i \otimes \boldsymbol{G}^i \tag{14}$$

so that the total deformation gradient (3) may be written in the form

$$\boldsymbol{F} = \boldsymbol{g}_i \otimes \boldsymbol{G}^i, \tag{15}$$

where the contravariant base vectors $\boldsymbol{G}^i$ are defined by $\boldsymbol{G}_i \cdot \boldsymbol{G}^j = \delta_i^j$. Variation of the deformation gradient yields

$$\delta \boldsymbol{F} = \delta \boldsymbol{g}_i \otimes \boldsymbol{G}^i \qquad \text{with} \qquad \delta \boldsymbol{g}_i = \delta \boldsymbol{x}_{,i} + \delta \tilde{\boldsymbol{g}}_i. \tag{16}$$

Introducing the expression of the inverse deformation gradient $\boldsymbol{F}^{-1} = \boldsymbol{G}_i \otimes \boldsymbol{g}^i$, one observes that

$$\delta \boldsymbol{F}^T \boldsymbol{F} = \delta \boldsymbol{g}_i \cdot \boldsymbol{g}_k \, \boldsymbol{G}^i \otimes \boldsymbol{G}^k \qquad \text{and} \qquad \delta \boldsymbol{F} \boldsymbol{F}^{-1} = \delta \boldsymbol{g}_i \otimes \boldsymbol{g}^i. \tag{17}$$

Together with $\delta \boldsymbol{F} = \text{Grad}[\delta \boldsymbol{u}] + \delta \tilde{\boldsymbol{H}}$ and (8), the internal virtual work (7) can be written in the form

$$G_{int} = \iiint \delta \boldsymbol{g}_i \cdot \boldsymbol{g}_j \hat{S}^{ij} \sqrt{G} d\theta^1 d\theta^2 d\theta^3 \tag{18}$$

where $\sqrt{G} = \boldsymbol{G}_1 \cdot (\boldsymbol{G}_2 \times \boldsymbol{G}_3)$, so that a volume element of the reference configuration $\mathcal{B}_0$ can be obtained via $dV = \sqrt{G} d\theta^1 d\theta^2 d\theta^3$. Using equations (12) and (16), G_{int} may now be written in the form

$$\boxed{G_{int} = \iiint \left\{ \delta \boldsymbol{x}_{,i} \cdot \boldsymbol{x}_{,j} + \delta \boldsymbol{x}_{,i} \cdot \tilde{\boldsymbol{g}}_j + \delta \tilde{\boldsymbol{g}}_i \cdot \boldsymbol{x}_{,j} + \delta \tilde{\boldsymbol{g}}_i \cdot \tilde{\boldsymbol{g}}_j \right\} \hat{S}^{ij} \sqrt{G} d\theta^1 d\theta^2 d\theta^3} \tag{19}$$

The virtual work contributions (equations (19), (4) and (5)) form the variational foundation of the proposed nonlinear 4-node shell element described in the next section.

3. Extensible Shell Formulation

We start from the essential kinematic assumption of a single director extensible shell kinematic which leads to the compatible finite element interpolations of the mid-surface and the extensible director field. Then we present two discontinuous EAS-expansions of the material displacement gradient which lead to enhanced covariant base vectors $\widetilde{\boldsymbol{g}}_i$. The aim of $\widetilde{\boldsymbol{g}}_3$ is to enrich the compatible transverse normal strain field and can be motivated by an extension of the underlying extensible shell kinematic. Additionally, the proposed expansion of the enhanced covariant base vectors $\widetilde{\boldsymbol{g}}_\alpha$ improves the membrane part of the bilinear shell element, particularly in bending dominated situtations and in the incompressible limit.

3.1. Kinematic Shell Assumptions

The formulation of the finite shell element is based on the three-dimensional continuum theory, where the placement of a point in shell space of the deformed configuration $\mathcal{B}$ is restricted by the assumption of a single *extensible* director kinematic

$$\boldsymbol{x}(\theta^i) = \varphi(\theta^\alpha) + \zeta \boldsymbol{d}(\theta^\alpha). \tag{20}$$

Here, $\varphi(\theta^\alpha)$ denotes the position vector of the actual shell mid-surface $\mathcal{M}$ labeled with curvilinear coordinates θ^α. Furthermore, $\theta^3 = \zeta \in [-h_0/2, h_0/2]$ describes the

coordinate in the thickness direction, where h_0 is the shell thickness of the reference configuration. The extensible director field $\boldsymbol{d}(\theta^\alpha)$ accounts for deformation dependent thickness stretch $\lambda = \|\boldsymbol{d}\| = h/h_0$ and allows for transverse shearing.

The corresponding quantities of the reference configuration $\mathcal{B}_0$ are denoted by capital letters. Here, the position vector $\boldsymbol{X}(\theta^i)$ of any point $P \in \mathcal{B}_0$ is defined by

$$\boldsymbol{X}(\theta^i) = \boldsymbol{\Phi}(\theta^\alpha) + \zeta \boldsymbol{D}(\theta^\alpha), \tag{21}$$

where $\boldsymbol{\Phi}(\theta^\alpha)$ denotes a configuration of the reference shell mid-surface $\mathcal{M}_0$. A director $\boldsymbol{D}(\theta^\alpha)$ of the initial configuration is defined as a unit vector perpendicular to the shell mid-surface $\mathcal{M}_0$. The kinematic quantities φ and $\boldsymbol{d}$ are approximated by means of compatible finite element interpolations of the corresponding nodal quantities as described in section 3.6. There, it will be shown that the bilinear approximation of the extensible director field requires special attention.

3.2. *EAS-Extension of Compatible Shell Kinematics*

We propose a discontinuous expansion of the material displacement gradient which can be motivated by higher order shell kinematics. Consider the expression

$$\tilde{\boldsymbol{H}} = \tilde{\boldsymbol{g}}_3 \otimes \boldsymbol{G}^3 \tag{22}$$

of the enhanced material displacement gradient, with the following discontinuous expansion of the enhanced covariant base vector

$$\tilde{\boldsymbol{g}}_3 = \zeta \tilde{\gamma} \boldsymbol{d}. \tag{23}$$

Here, $\tilde{\gamma}(\boldsymbol{\xi})$ describes the expansion which is based on the natural coordinates $\boldsymbol{\xi} = [\xi^1, \xi^2]$ of the isoparamatric domain $\square = [-1, 1] \times [-1, 1]$:

$$\tilde{\gamma} = \boldsymbol{e}^T \boldsymbol{\Gamma}_d \quad \text{with} \quad \boldsymbol{e}^T = [1,\ \xi^1,\ \xi^2,\ \xi^1\xi^2] \quad \text{and} \quad \boldsymbol{\Gamma}_d = [\Gamma_d^1,\ \Gamma_d^2,\ \Gamma_d^3,\ \Gamma_d^4]^T. \tag{24}$$

Accordingly, $\boldsymbol{\Gamma}_d$ contains four internal degrees of freedom associated with the interpolation vector $\boldsymbol{e}(\boldsymbol{\xi})$ which defines the interpolation in the isoparametric domain $\square$. The total covariant base vector $\boldsymbol{g}_3$ can now be composed of the compatible part $\boldsymbol{x}_{,3}$ which follows from (20) and the enhanced part (23) so that

$$\boldsymbol{g}_3 = \boldsymbol{x}_{,3} + \tilde{\boldsymbol{g}}_3 = (1 + \zeta \tilde{\gamma}) \boldsymbol{d}. \tag{25}$$

The condition (6) requires that

$$\iiint \tilde{\boldsymbol{g}}_3 \otimes \boldsymbol{G}^3 \sqrt{G} d\theta^1 d\theta^2 d\theta^3 = \int_{\square} \left[\int_{-h_0/2}^{h_0/2} \zeta \, d\zeta \right] \tilde{\gamma} \boldsymbol{d} \otimes \boldsymbol{D} \sqrt{A} d\square = \boldsymbol{0}. \tag{26}$$

This condition is satisfied, since the term in the square bracket is zero. For the sake of simplicity, it has been assumed in (26) that the metric of the initial shell space $\mathcal{B}_0$ coincides with the metric of the initial mid-surface $\mathcal{M}_0$, i.e. $\sqrt{G} = \sqrt{A} = \|\boldsymbol{\Phi}_{,1} \times \boldsymbol{\Phi}_{,2}\|$ which is justified for thin shells.

Remark. The expansion (23) for $\widetilde{\boldsymbol{g}}_3$ can be motivated by means of higher order shell kinematics. According to Naghdi [24] (page 466) a shell theory can be derived from three-dimensional continuum mechanics using the following series for the position vector of the deformed shell configuration

$$\boldsymbol{x}(\theta^i) = \boldsymbol{\varphi}(\theta^\alpha) + \sum_{N=1}^{\infty} \zeta^N \boldsymbol{d}_N(\theta^\alpha). \tag{27}$$

The applied (compatible) single extensible director kinematic (20) follows from (27) by setting $N = 1$ and $\boldsymbol{d}_1 = \boldsymbol{d}$. Thus the higher order terms with $N \geq 2$ are truncated. If we now consider the quadratic term ($N = 2$) with

$$\widetilde{\boldsymbol{x}}(\theta^i) = \zeta^2 \boldsymbol{d}_2(\theta^\alpha) \qquad \text{and} \qquad \boldsymbol{d}_2 = \frac{1}{2}\widetilde{\gamma}\boldsymbol{d}, \tag{28}$$

the corresponding covariant base vector $\widetilde{\boldsymbol{g}}_3$ is given by

$$\widetilde{\boldsymbol{g}}_3 = \widetilde{\boldsymbol{x}}_{,3} = \zeta\widetilde{\gamma}\boldsymbol{d}. \tag{29}$$

3.3. EAS-Improvement of Membrane Part

The performance of the extensible bilinear shell element can be further improved with the help of the EAS method, especially for in-plane bending dominated cases and the incompressible limit. To this end we consider the following expansion of the enhanced material displacement gradient

$$\tilde{\boldsymbol{H}} = \widetilde{\boldsymbol{\varphi}}_\alpha \otimes \boldsymbol{G}^\alpha \tag{30}$$

with discontinuous enhanced covariant base vectors

$$\widetilde{\boldsymbol{g}}_\alpha = \widetilde{\boldsymbol{\varphi}}_\alpha = \sum_{J=1}^{2} a_\alpha^J \Gamma_J^\beta \boldsymbol{\varphi}_{0,\beta} \qquad \text{and} \qquad a_\alpha^J = \frac{\sqrt{A_0}}{\sqrt{A}} \xi^J (\boldsymbol{G}_0^J \cdot \boldsymbol{G}_\alpha). \tag{31}$$

In (31), for all expressions with the subscript $_0$ the corresponding quantity has to be evaluated in the center of the element, i.e. at $\boldsymbol{\xi} = \boldsymbol{0}$ and $\zeta = 0$. Furthermore, Γ_J^β denote four internal degrees of freedom. The proposed expansion (31) of the enhanced covariant base vectors $\widetilde{\boldsymbol{g}}_\alpha$ can be derived from Wilson's incompatible shape functions (Wilson et al. [25])

$$\tilde{N}^J = \frac{1}{2}\left\{(\xi^J)^2 - 1\right\} \qquad (J = 1, 2). \tag{32}$$

To this end, we use the systematic procedure for the design of interpolations for the enhanced displacement gradient as suggested by Simo, Armero & Taylor [26] which can be applied within the curvilinear formulation as follows.

Define the map $\mathbb{H}$ on the isoparametric domain $\square$ by the interpolation formula

$$\mathbb{H}(\xi^\alpha) = \sum_{J=1}^{2} \boldsymbol{\Gamma}_J \otimes \mathrm{Grad}_\xi[\tilde{N}^J], \tag{33}$$

where $\boldsymbol{\Gamma}_J = [\Gamma_J^1,\ \Gamma_J^2,\ 0]$ contains two internal degrees of freedom which correspond to each incompatible shape function (32). Then calculate the enhanced material displacement gradient according to the formula

$$\tilde{\boldsymbol{H}} = \frac{\sqrt{A_0}}{\sqrt{A}} \bar{\boldsymbol{F}}_0 \boldsymbol{J}_0 \mathbb{H}(\xi^\alpha) \boldsymbol{J}_0^{-1}, \tag{34}$$

where $\bar{\boldsymbol{F}}_0$ denotes the compatible deformation gradient evaluated at the center of the element

$$\bar{\boldsymbol{F}}_0 = \mathrm{Grad}_0[\boldsymbol{x}(\xi^i)] = \boldsymbol{x}_{0,i} \otimes \boldsymbol{G}_0^i \tag{35}$$

and $\boldsymbol{J}_0$ is the constant reference Jacobian, evaluated at the center of the element, so that

$$\boldsymbol{J}_0 = \boldsymbol{G}_{0i} \otimes \boldsymbol{e}_i \quad \text{and} \quad \boldsymbol{J}_0^{-1} = \boldsymbol{e}_i \otimes \boldsymbol{G}_0^i. \tag{36}$$

Introducing equations (33), (35) and (36) into (34) yields

$$\tilde{\boldsymbol{H}} = \sum_{J=1}^{2} \frac{\sqrt{A_0}}{\sqrt{A}} \frac{\partial \tilde{N}^J}{\partial \xi^\alpha} \Gamma_J^\beta \boldsymbol{x}_{0,\beta} \otimes \boldsymbol{G}_0^\alpha. \tag{37}$$

After introduction of the appropriate assumption for the bilinear shell element $\boldsymbol{G}_3 \cdot \boldsymbol{G}_0^\alpha = 0$ and realizing that $\tilde{N}_{,\alpha}^J = \xi^J \delta_\alpha^J$, one eventually obtains the proposed expansion (30) for the enhanced material displacement gradient

$$\tilde{\boldsymbol{H}} = \sum_{J=1}^{2} a_\alpha^J \Gamma_J^\beta \boldsymbol{\varphi}_{0\beta} \otimes \boldsymbol{G}^\alpha = \tilde{\boldsymbol{\varphi}}_\alpha \otimes \boldsymbol{G}^\alpha \tag{38}$$

with a_α^J from equation $(31)_2$. The condition (6) in combination with (34) leads to

$$\int_{\mathcal{B}_0} \tilde{\boldsymbol{H}}\, dV = \sqrt{A_0} h_0 \bar{\boldsymbol{F}}_0 \boldsymbol{J}_0 \int_{\square} \mathbb{H}(\xi^\alpha)\, d\square\, \boldsymbol{J}_0^{-1} = \boldsymbol{0} \tag{39}$$

and is automatically satisfied due to the nature of $\mathbb{H}(\xi^\alpha)$, since the restriction

$$\int_{\square} \mathbb{H}(\xi^\alpha)\, d\square = \boldsymbol{0} \tag{40}$$

holds in view of equation (33). The total covariant base vectors $\boldsymbol{g}_\alpha$ can now be obtained from the compatible part $\boldsymbol{x}_{,\alpha}$ which follows from the shell kinematic (20) in conjunction with the enhanced part $(31)_1$, so that

$$\boldsymbol{g}_\alpha = \boldsymbol{x}_{,\alpha} + \tilde{\boldsymbol{g}}_\alpha = \boldsymbol{\psi}_\alpha + \zeta \boldsymbol{d}_{,\alpha}, \tag{41}$$

where

$$\boldsymbol{\psi}_\alpha = \boldsymbol{\varphi}_{,\alpha} + \tilde{\boldsymbol{\varphi}}_\alpha. \tag{42}$$

Finally, from (22) and (30) we obtain the total enhanced material displacement gradient which can be written in the form

$$\boxed{\tilde{\boldsymbol{H}} = \widetilde{\boldsymbol{\varphi}}_{\alpha} \otimes \boldsymbol{G}^{\alpha} + \zeta \tilde{\gamma} \boldsymbol{d} \otimes \boldsymbol{G}^{3}} \tag{43}$$

By using definition (3), i.e. $\boldsymbol{F} = \mathrm{Grad}_X[\boldsymbol{x}] + \tilde{\boldsymbol{H}}$, and introducing the extensible shell kinematic (20), the total deformation gradient of the proposed shell formulation is now given by

$$\boxed{\boldsymbol{F} = \{\boldsymbol{\psi}_{\alpha} + \zeta \boldsymbol{d}_{,\alpha}\} \otimes \boldsymbol{G}^{\alpha} + \{1 + \zeta \widetilde{\gamma}\} \boldsymbol{d} \otimes \boldsymbol{G}^{3}} \tag{44}$$

The corresponding covariant components of the local metric tensor can be calculated via $g_{ij} = \boldsymbol{G}_i \cdot (\boldsymbol{F}^T \boldsymbol{F}) \boldsymbol{G}_j$. Subsequent ordering of the components with respect to the thickness coordinate ζ leads to

$$g_{ij} = g_{ij}^{\{0\}} + \zeta g_{ij}^{\{1\}} + \zeta^2 g_{ij}^{\{2\}} \tag{45}$$

with

$$\begin{aligned}
g_{\alpha\beta}^{\{0\}} &= \boldsymbol{\psi}_{\alpha} \cdot \boldsymbol{\psi}_{\beta}, & g_{\alpha\beta}^{\{1\}} &= \boldsymbol{d}_{,\alpha} \cdot \boldsymbol{\psi}_{\beta} + \boldsymbol{\psi}_{\alpha} \cdot \boldsymbol{d}_{,\beta}, & g_{\alpha\beta}^{\{2\}} &= \boldsymbol{d}_{,\alpha} \cdot \boldsymbol{d}_{,\beta}, \\
g_{3\alpha}^{\{0\}} &= \boldsymbol{\psi}_{\alpha} \cdot \boldsymbol{d}, & g_{3\alpha}^{\{1\}} &= \boldsymbol{d} \cdot \boldsymbol{d}_{,\alpha} + \widetilde{\gamma} \boldsymbol{\psi}_{\alpha} \cdot \boldsymbol{d}, & g_{3\alpha}^{\{2\}} &= \widetilde{\gamma} \boldsymbol{d} \cdot \boldsymbol{d}_{,\alpha}, \\
g_{33}^{\{0\}} &= \boldsymbol{d} \cdot \boldsymbol{d}, & g_{33}^{\{1\}} &= 2 \widetilde{\gamma} \boldsymbol{d} \cdot \boldsymbol{d}, & g_{33}^{\{2\}} &= \widetilde{\gamma}^2 \boldsymbol{d} \cdot \boldsymbol{d}
\end{aligned} \tag{46}$$

along with analogous expressions for $G_{ij} = \boldsymbol{G}_i \cdot \boldsymbol{G}_j$ which follow directly from the kinematic assumption (21) for the reference configuration. The state of deformation can now be described using the Green-Lagrangian strain tensor

$$\boldsymbol{E} = \frac{1}{2} (g_{ij} - G_{ij}) \boldsymbol{G}^i \otimes \boldsymbol{G}^j, \tag{47}$$

which may be written analogous to (45) in partitioned form

$$\boldsymbol{E} = \boldsymbol{E}^{\{0\}} + \zeta \boldsymbol{E}^{\{1\}} + \zeta^2 \boldsymbol{E}^{\{2\}}. \tag{48}$$

Accordingly, the covariant thickness strains which are constant across the shell thickness yield

$$E_{33}^{\{0\}} = \frac{1}{2} \{ \|\boldsymbol{d}\|^2 - 1 \}, \tag{49}$$

whereas the corresponding linear part may be written in the form

$$E_{33}^{\{1\}} = \tilde{\gamma} \|\boldsymbol{d}\|^2. \tag{50}$$

Equation (50) indicates that the EAS-interpolation of the covariant base vector $\widetilde{\boldsymbol{g}}_3$ leads to thickness strains which are linear across the shell thickness. Thus, three-dimensional constitutive models can be implemented without any shell-specific modifications.

3.4. Stress-Resultant Weak Form

We derive the stress-resultant counterpart of the EAS-weak form (1) based on the curvilinear representation (19). To this end we define stress-resultants from the three-dimensional theory. The stress across the coordinate surface $\theta^i = \text{constant}$ can be represented by a stress vector (see Green & Zerna [27])

$$\boldsymbol{t}^i = \frac{\boldsymbol{T}^i}{\sqrt{g g^{ii}}} \qquad \text{with} \qquad \boldsymbol{T}^i = \sqrt{g}\sigma^{ik}\boldsymbol{g}_k = \sqrt{g}\boldsymbol{\sigma}\boldsymbol{g}^i, \tag{51}$$

where $\boldsymbol{\sigma}$ denotes the Cauchy stress tensor, so that $\sqrt{g}\boldsymbol{\sigma} = \sqrt{G}\boldsymbol{\tau}$. With the help of (10) we now define

$$\hat{\boldsymbol{T}}^i = \sqrt{G}\hat{\boldsymbol{\tau}}\boldsymbol{g}^i = \sqrt{G}\hat{S}^{ik}\boldsymbol{g}_k. \tag{52}$$

Introducing (52) into the internal virtual work (18) of the EAS-formulation yields

$$G_{int} = \int\!\!\int\!\!\int \left\{\delta\boldsymbol{g}_\alpha \cdot \hat{\boldsymbol{T}}^\alpha + \delta\boldsymbol{g}_3 \cdot \hat{\boldsymbol{T}}^3\right\} d\theta^1 d\theta^2 d\theta^3, \tag{53}$$

where the variation of the total covariant base vectors (25) and (41) is given by

$$\begin{aligned} \delta\boldsymbol{g}_3 &= \delta\boldsymbol{d} + \zeta\delta\widetilde{\boldsymbol{d}}, \\ \delta\boldsymbol{g}_\alpha &= \delta\boldsymbol{\psi}_\alpha + \zeta\delta\boldsymbol{d}_{,\alpha}, \end{aligned} \tag{54}$$

and $\widetilde{\boldsymbol{d}} = \tilde{\gamma}\boldsymbol{d}$. Further, we define the stress-resultants $\hat{\boldsymbol{n}}^i$ and $\hat{\boldsymbol{m}}^i$ by

$$\hat{\boldsymbol{n}}^i = \frac{1}{\sqrt{a}}\int_{-\frac{h_0}{2}}^{\frac{h_0}{2}} \hat{\boldsymbol{T}}^i \, d\zeta, \qquad \hat{\boldsymbol{m}}^i = \frac{1}{\sqrt{a}}\int_{\frac{-h_0}{2}}^{\frac{h_0}{2}} \zeta\hat{\boldsymbol{T}}^i \, d\zeta. \tag{55}$$

Introducing (54) and (55) into the internal virtual work (53) leads to the corresponding stress-resultant expression

$$G_{int} = \sum_{e=1}^{n_{elem}} \int_\square \left\{\hat{\boldsymbol{n}}^\alpha \cdot \delta\boldsymbol{\psi}_\alpha + \hat{\boldsymbol{m}}^\alpha \cdot \delta\boldsymbol{d}_{,\alpha} + \hat{\boldsymbol{n}}^3 \cdot \delta\boldsymbol{d} + \hat{\boldsymbol{m}}^3 \cdot \delta\widetilde{\boldsymbol{d}}\right\} \sqrt{a}\, d\square, \tag{56}$$

where n_{elem} denotes the number of finite shell elements used for the discretization of the continuous problem. If we drop the contributions of the proposed EAS-expansions for $\widetilde{\boldsymbol{\varphi}}_\alpha$ and $\widetilde{\boldsymbol{g}}_3$, equations (31) and (23), so that $\widetilde{\boldsymbol{d}} = \boldsymbol{0}$ and $\boldsymbol{\psi}_\alpha = \boldsymbol{\varphi}_{,\alpha}$, then the virtual work of the stress-resultants (56) coincides with the corresponding expression used by Simo, Rifai & Fox [7] (equation (2.14a)). The main advantage of the present formulation lies in the appearance of the fourth term in (56) which arises from the extension of the underlying extensible shell kinematic (20) by means of the enhanced covariant base vector $\widetilde{\boldsymbol{g}}_3$, equation (23). Because of this additional term, complete three-dimensional constitutive models can be applied without any modifications. In contrast, the bending part of the constitutive model in [7] needs to be modified by the zero normal stress assumption.

Based on the resultant expression (56) one may proceed with the definition of (symmetric) effective stress resultants as e.g. in [7]. Alternatively, the definition of stress resultants can be avoided when the stress components of the continuum theory are employed directly. Consequently, a formulation that is ideally suited for the numerical implementation of various three-dimensional constitutive models can be obtained.

3.5. *Weak Form Based on Stress Components*

We proceed directly from the three-dimensional curvilinear representation (19) of the EAS-formulation. With the help of the covariant components of the metric tensor which are given by (45), equation (19) may be rewritten for one element

$$G^e_{int} = \frac{1}{2}\int_{\square} \left\{ \delta g^{\{0\}}_{ij}\, \hat{S}^{ij}_{\{0\}} + \delta g^{\{1\}}_{ij}\, \hat{S}^{ij}_{\{1\}} + \delta g^{\{2\}}_{ij}\, \hat{S}^{ij}_{\{2\}} \right\} d\square, \tag{57}$$

where the integration across the shell thickness is confined to the constitutive expressions

$$\hat{S}^{ij}_{\{N\}} = \int_{-\frac{h_0}{2}}^{\frac{h_0}{2}} \zeta^N \hat{S}^{ij} \sqrt{G}\, d\zeta \tag{58}$$

for $N = 0, 1, 2$. Here, $\hat{S}^{ij}$ are the contravariant components of the stress tensor (9) which can be calculated with the help of the strain energy function W. Depending on the three-dimensional constitutive model, the integration across the shell thickness in (58) can be carried out analytically or has to be performed numerically.

For the sake of an efficient numerical implementation, we neglect in (57) $g^{\{2\}}_{33}$ as well as the contributions of the EAS-expansion to the transverse shear strains. Numerical simulations confirm that these terms only play a negligible part. With the help of (46) equation (57) may now be written in the final form

$$\begin{aligned} G^e_{int} = \int_{\square} \Big\{ & \delta\boldsymbol{\psi}_\alpha \cdot \boldsymbol{\psi}_\beta \hat{S}^{\alpha\beta}_{\{0\}} + (\delta\boldsymbol{\varphi}_{,\alpha} \cdot \boldsymbol{d} + \delta\boldsymbol{d} \cdot \boldsymbol{\varphi}_{,\alpha}) \hat{S}^{\alpha 3}_{\{0\}} + \delta\boldsymbol{d} \cdot \boldsymbol{d}\, \hat{S}^{33}_{\{0\}} \\ & + (\delta\boldsymbol{\psi}_\alpha \cdot \boldsymbol{d}_{,\beta} + \delta\boldsymbol{d}_{,\alpha} \cdot \boldsymbol{\psi}_\beta) \hat{S}^{\alpha\beta}_{\{1\}} + (\delta\boldsymbol{d} \cdot \boldsymbol{d}_{,\alpha} + \delta\boldsymbol{d}_{,\alpha} \cdot \boldsymbol{d}) \hat{S}^{\alpha 3}_{\{1\}} \\ & + (2\widetilde{\gamma}\delta\boldsymbol{d} \cdot \boldsymbol{d} + \delta\widetilde{\gamma}\|\boldsymbol{d}\|^2) \hat{S}^{33}_{\{1\}} + \delta\boldsymbol{d}_{,\alpha} \cdot \boldsymbol{d}_{,\beta} \hat{S}^{\alpha\beta}_{\{2\}} \Big\}\, d\square. \end{aligned} \tag{59}$$

Expression (59) leads to an extensible shell formulation which is ideally suited for the implementation of three-dimensional nonlinear constitutive models. Next, we deal with the remaining compatible finite element interpolations of the mid-surface and the extensible director field.

3.6. *Compatible Interpolations*

According to the isoparametric concept (see e.g. Hughes [28]), the position vector $\boldsymbol{\varphi}(\xi^\alpha)$ of the mid-surface as well as the extensible director $\boldsymbol{d}(\xi^\alpha)$ are interpolated with the help of the standard bilinear shape functions N^I: $\square \to \mathbb{R}$. Within one element the position vector of the mid-surface is given by

$$\boldsymbol{\varphi}(\xi^\alpha) = \sum_{I=1}^{4} N^I(\xi^\alpha) \boldsymbol{\varphi}_I. \tag{60}$$

Interpolation of the director field. The approximation of the extensible director field within the discrete formulation requires special attention in order to obtain a good numerical performance in the thin-shell limit. The simplest kind of parametrization relies

on the direct interpolation of the components of the nodal extensible directors $\boldsymbol{d}_I$

$$\boldsymbol{d}(\xi^\alpha) = \sum_{I=1}^{4} N^I(\xi^\alpha)\boldsymbol{d}_I. \tag{61}$$

The simplicity of this formulation is due to the additive structure of the update $\boldsymbol{d}^{(k+1)} = \boldsymbol{d}^{(k)} + \Delta\boldsymbol{d}$ within an iterative solution procedure. Accordingly, the interpolation (61) does not require any rotational variables defining a rotation tensor. However, as has been shown by Simo, Rifai & Fox [7], the formulation suffers from pathological behavior in the thin-shell limit. As shown below this is due to the appearance of parasitic thickness strains induced by interpolation (61) in the case of curved shells.

Another parametrization of the director field is based on a multiplicative split into an extensible and inextensible part

$$\boldsymbol{d}(\xi^\alpha) = \lambda(\xi^\alpha)\,\boldsymbol{t}(\xi^\alpha). \tag{62}$$

Therefore, the thickness stretch $\lambda = h/h_0$ and the director orientation characterized by the unit vector $\boldsymbol{t}$ are kinematically decoupled. According to the constraint $\|\boldsymbol{t}\| = 1$, a rotation tensor has to be used as in shell formulations based on the zero normal stress condition and inextensibility in the thickness direction. The structure of the multiplicative decomposition (62) is preserved in the discrete model with interpolations

$$\lambda(\xi^\alpha) = \sum_{I=1}^{4} N^I(\xi^\alpha)\lambda_I \qquad \text{and} \qquad \Delta\boldsymbol{t}(\xi^\alpha) = \sum_{I=1}^{4} N^I(\xi^\alpha)\Delta\boldsymbol{t}_I. \tag{63}$$

Application of interpolations (63) leads to a numerical formulation that recovers a plane stress response in the thin-shell limit without any numerical problems, as has been shown in Betsch, Gruttmann & Stein [11].

A third description for the discrete extensible director field relies on the interpolation (61) in combination with the multiplicative decomposition (62) of the nodal director vectors

$$\boldsymbol{d}(\xi^\alpha) = \sum_{I=1}^{4} N^I(\xi^\alpha)\lambda_I\boldsymbol{t}_I. \tag{64}$$

Remarkably, numerical simulations with this kind of director interpolation yield identical results when compared with the less elaborate interpolation formula (61). This indicates that the simple *nodal* director update procedure $\boldsymbol{d}_I^{(k+1)} = \boldsymbol{d}_I^{(k)} + \Delta\boldsymbol{d}_I$ is equivalent to the more elaborate nodal update for the multiplicative decomposition which requires an orthogonal matrix $\Delta\boldsymbol{\Lambda}_I$ in order to achieve $\boldsymbol{t}_I^{(k+1)} = \Delta\boldsymbol{\Lambda}_I\boldsymbol{t}_I^{(k)}$.

In the next section we consider the discrete director field associated with interpolation (61) which causes the pathological behavior in the thin-shell limit.

3.6.1. One-Dimensional Model Problem. In order to examine the behavior of the interpolation (61) of the director field, it is sufficient to consider the one-dimensional model problem depicted in Fig. 1. We consider a cut through a curved shell structure with corresponding finite element discretization. The shell mid-surface $\varphi(\xi)$ and the

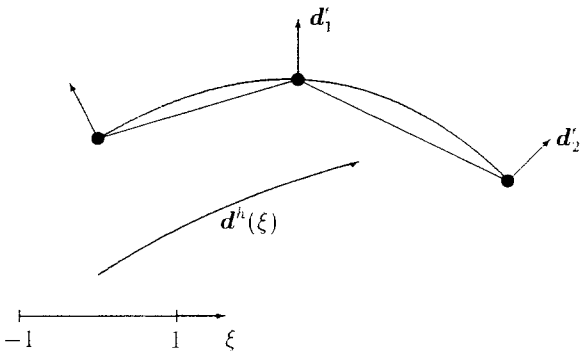

Fig. 1. Cut through a curved shell with discretization.

extensible director field $\boldsymbol{d}(\xi)$ are approximated by piecewise-linear interpolations of the nodal vectors $\varphi_I = \varphi(\xi_I)$ and $\boldsymbol{d}_I = \boldsymbol{d}(\xi_I)$, respectively.

Accordingly, for one representative element one obtains the discrete extensible director field

$$\boldsymbol{d}^h(\xi) = \frac{1}{2}(1-\xi)\boldsymbol{d}_1^e + \frac{1}{2}(1+\xi)\boldsymbol{d}_2^e. \tag{65}$$

For the limiting case of a thin shell we consider pure bending deformation, where the inextensibility condition $\boldsymbol{d}\cdot\boldsymbol{d} = 1$ holds along with $E_{33}^{\{0\}} = 0$. Moreover, we assume for the discrete model that the inextensibility condition is fulfilled at the nodal points, i.e. $\|\boldsymbol{d}_1^e\| = 1$ and $\|\boldsymbol{d}_2^e\| = 1$. Application of the interpolation (65) yields

$$\boldsymbol{d}^h\cdot\boldsymbol{d}^h = 1 + \frac{1}{2}(1-\xi^2)(\boldsymbol{d}_1^e\cdot\boldsymbol{d}_2^e - 1). \tag{66}$$

Thus, for the discrete director field the inextensibility condition holds only if $\boldsymbol{d}_1^e\cdot\boldsymbol{d}_2^e = 1$, i.e. in the case of no curvature. In general the interpolation of the director vector (65) induces thickness change and, therefore, artificial thickness strains which are constant over the shell thickness. Obviously, this defect depends on the curvature and on the mesh density.

Furthermore, for the linearization of the discrete thickness strains one obtains

$$\delta E_{33}^{\{0\}} = \boldsymbol{d}^h\cdot\delta\boldsymbol{d}^h = \frac{1}{4}(1-\xi^2)(\boldsymbol{d}_1^e\cdot\delta\boldsymbol{d}_2^e + \boldsymbol{d}_2^e\cdot\delta\boldsymbol{d}_1^e) \tag{67}$$

which indicates once more that, even in the case of linear elasticity and initial curvature, artificial straining occurs. Consequently, any bending deformation of the element is accompanied by thickness stretching, thus increasing the bending stiffness. Numerical experiments show that the defect of the interpolation (65) leads to locking response in the case of curved shells. Locking worsens with greater curvature (initial or deformation dependent), especially for coarse meshes.

3.6.2. Assumed Strain Interpolation of $E_{33}^{\{0\}}$. To circumvent the effect of artificial thickness strains, we employ an assumed strain approximation for the covariant com-

ponent $E_{33}^{\{0\}}$ of the Green-Lagrangian strain tensor. We assume bilinear interpolations of the thickness strain field, where the element nodes serve as sampling points of the compatible thickness strains. Accordingly, we obtain a C^0-continuous strain field of the form

$$\tilde{E}_{33}^{\{0\}}(\xi^\alpha) = \sum_{I=1}^{4} N^I(\xi^\alpha) E_{33}^{\{0\}}(\xi_I^\alpha), \tag{68}$$

with the compatible nodal thickness strains (49)

$$E_{33}^{\{0\}}(\xi_I^\alpha) = \frac{1}{2}(\boldsymbol{d}_I \cdot \boldsymbol{d}_I - 1). \tag{69}$$

Variation of equation (68) yields the contribution to the linearized discrete strain-nodal operator matrix

$$\delta \tilde{E}_{33}^{\{0\}}(\xi^\alpha) = \sum_{I=1}^{4} N^I(\xi^\alpha) \boldsymbol{d}_I^T \delta \boldsymbol{d}_I. \tag{70}$$

Furthermore, for the contribution to the geometric part of the tangent stiffness matrix, one obtains

$$\Delta\delta \tilde{E}_{33}^{\{0\}}(\xi^\alpha) = \sum_{I=1}^{4} \Delta \boldsymbol{d}_I^T N^I(\xi^\alpha) \mathbf{1} \delta \boldsymbol{d}_I. \tag{71}$$

Accordingly the proposed assumed strain interpolation (68) is easy to implement and makes the simple interpolation of the extensible director (61) competitive with more involved formulations that need rotational degrees of freedom.

3.6.3. Assumed Strain Interpolation of $E_{\alpha 3}^{\{0\}}$. The well-known shear locking effect of low order C^0-continuous shell formulations can also be eliminated by means of an assumed strain modification. For the present bilinear shell element we modify the discrete compatible transverse shear strains $E_{\alpha 3}^{\{0\}}$ introducing the assumed strain interpolation of Dvorkin & Bathe [17] (see equation (105) in Appendix A.1), which has been further investigated by Stander, Matzenmiller & Ramm [19] and Parisch [20].

3.7. Implementation Aspects

In order to obtain an efficient numerical implementation, proceeding from expression (59) is suggested, since the explicit integration across the shell thickness is confined to the constitutive terms, i.e. the stress components and the tangent moduli, and can be performed outside the nodal loops. However, for the sake of maximum clearness, we proceed from the implicit version

$$G_{int}^e = \int_{\square} \int_{-\frac{h_0}{2}}^{\frac{h_0}{2}} \Big[\delta \boldsymbol{g}_\alpha \cdot \boldsymbol{g}_\beta \hat{S}^{\alpha\beta} + \{\delta \boldsymbol{x}_{,\alpha} \cdot \boldsymbol{d} + \delta \boldsymbol{d} \cdot \boldsymbol{x}_{,\alpha}\} \hat{S}^{\alpha 3} + \{\delta \boldsymbol{d} \cdot \boldsymbol{d}(1 + \zeta 2\tilde{\gamma}) + \delta\tilde{\gamma}\zeta \|\boldsymbol{d}\|^2\} \hat{S}^{33} \Big] \sqrt{G}\, d\zeta\, d\square \tag{72}$$

which is equivalent to (59), as can be shown by introducing equations (41) and (20) into (72). It is a straightforward way to obtain the corresponding explicit version by ordering with respect to the powers of the thickness coordinate ζ. Introduction of the compatible and enhanced interpolations into (72) leads to the discrete expression

$$G^e_{int} = \delta \boldsymbol{v}_e^T \int_{\square} \int_{-\frac{h_0}{2}}^{\frac{h_0}{2}} \boldsymbol{B}^T \widehat{\boldsymbol{S}} \sqrt{G}\, d\zeta\, d\square + \delta \boldsymbol{\Gamma}_e^T \int_{\square} \int_{-\frac{h_0}{2}}^{\frac{h_0}{2}} \widetilde{\boldsymbol{B}}^T \widehat{\boldsymbol{S}} \sqrt{G}\, d\zeta\, d\square. \tag{73}$$

In (73) $\boldsymbol{v}_e^T = [\boldsymbol{v}_1^T, ..., \boldsymbol{v}_4^T]$ contains the compatible nodal variables $\boldsymbol{v}_I^T = [\boldsymbol{\varphi}_I^T, \boldsymbol{d}_I^T]$, and $\boldsymbol{\Gamma}_e^T = [\boldsymbol{\Gamma}_d^T, \boldsymbol{\Gamma}_1^T, \boldsymbol{\Gamma}_2^T]$ contains the internal degrees of freedom. The symmetric components of the Green-Lagrangian strain tensor are ordered in the convenient column-matrix form

$$\boldsymbol{E} = [E_{11}, E_{22}, 2E_{12}, E_{33}, 2E_{13}, 2E_{23}]^T \tag{74}$$

along with the corresponding ordering of the stress components

$$\widehat{\boldsymbol{S}} = [\hat{S}^{11}, \hat{S}^{22}, \hat{S}^{12}, \hat{S}^{33}, \hat{S}^{13}, \hat{S}^{23}]^T. \tag{75}$$

The linearized strains are given by

$$\delta \boldsymbol{E} = \sum_{I=1}^{4} \boldsymbol{B}_I \delta \boldsymbol{v}_I + \widetilde{\boldsymbol{B}} \delta \boldsymbol{\Gamma}_e, \tag{76}$$

where $\boldsymbol{B}_I$ denotes the compatible nodal operator matrix and $\widetilde{\boldsymbol{B}}$ is the operator matrix of the internal degrees of freedom

$$\boldsymbol{B}_I = \begin{bmatrix} \boldsymbol{B}^{\varphi}_{I_{3\times 3}} & \boldsymbol{B}^{d}_{I_{3\times 3}} \\ \boldsymbol{0}_{1\times 3} & \boldsymbol{b}^{33}_{I_{1\times 3}} \\ \boldsymbol{B}^{S}_{\varphi\, I_{2\times 3}} & \boldsymbol{B}^{S}_{d\, I_{2\times 3}} \end{bmatrix} \quad \text{and} \quad \widetilde{\boldsymbol{B}} = \begin{bmatrix} \boldsymbol{0}_{3\times nt} & \widetilde{\boldsymbol{B}}^{m}_{1_{3\times 2}} & \widetilde{\boldsymbol{B}}^{m}_{2_{3\times 2}} \\ \widetilde{\boldsymbol{b}}^{33}_{1\times nt} & \boldsymbol{0}_{1\times 2} & \boldsymbol{0}_{1\times 2} \\ \boldsymbol{0}_{2\times nt} & \boldsymbol{0}_{2\times 2} & \boldsymbol{0}_{2\times 2} \end{bmatrix}. \tag{77}$$

The index nt denotes the number of internal degrees of freedom Γ_d^{nt} in (24). A detailed derivation of the submatrices in $\boldsymbol{B}_I$ and $\widetilde{\boldsymbol{B}}$ is contained in the Appendix A.1. Furthermore, in (73) $\boldsymbol{B} = [\boldsymbol{B}_1, \boldsymbol{B}_2, \boldsymbol{B}_3, \boldsymbol{B}_4]$. Linearization of the discretised static weak form (1)

$$\sum_{e=1}^{n_{elem}} G^e = \sum_{e=1}^{n_{elem}} \left[G^e_{int} - G^e_{ext} \right] = 0 \tag{78}$$

yields

$$\sum_{e=1}^{n_{elem}} \left[G^e + DG^e \cdot (\Delta \boldsymbol{v}_e,\ \Delta \boldsymbol{\Gamma}_e) \right] = 0 \tag{79}$$

and leads to an algebraic system of linear equations for the iterative solution procedure by means of Newton's method in combination with an elimination of the internal degrees of freedom on the element level. Accordingly, for a typical Newton iteration (79) may be written in the form

$$\sum_{e=1}^{n_{elem}} [\delta \boldsymbol{v}_e^T,\ \delta \boldsymbol{\Gamma}_e^T] \left\{ \begin{bmatrix} \boldsymbol{f}^e_{int} - \boldsymbol{f}^e_{ext} \\ \widetilde{\boldsymbol{f}}^e_{int} \end{bmatrix} + \begin{bmatrix} \boldsymbol{K}_{vv} & \boldsymbol{K}_{v\Gamma} \\ \boldsymbol{K}_{\Gamma v} & \boldsymbol{K}_{\Gamma\Gamma} \end{bmatrix} \begin{bmatrix} \Delta \boldsymbol{v}_e \\ \Delta \boldsymbol{\Gamma}_e \end{bmatrix} \right\} = 0. \tag{80}$$

Each submatrix of the Hessian matrix in (80) consists of a material and a geometric part. The derivation of the geometric part is described in the Appendix A.2. Accordingly, we obtain

$$\boldsymbol{K}_{vv} = \int_{\square}\int_{-\frac{h_0}{2}}^{\frac{h_0}{2}} \boldsymbol{B}^T \mathcal{C} \boldsymbol{B} \sqrt{G}\, d\zeta\, d\square + \boldsymbol{K}_{vv}^{geo}, \tag{81}$$

$$\boldsymbol{K}_{v\Gamma} = \int_{\square}\int_{-\frac{h_0}{2}}^{\frac{h_0}{2}} \boldsymbol{B}^T \mathcal{C} \widetilde{\boldsymbol{B}} \sqrt{G}\, d\zeta\, d\square + \boldsymbol{K}_{v\Gamma}^{geo}, \tag{82}$$

$$\boldsymbol{K}_{\Gamma v} = \boldsymbol{K}_{v\Gamma}^T, \tag{83}$$

$$\boldsymbol{K}_{\Gamma\Gamma} = \int_{\square}\int_{-\frac{h_0}{2}}^{\frac{h_0}{2}} \widetilde{\boldsymbol{B}}^T \mathcal{C} \widetilde{\boldsymbol{B}} \sqrt{G}\, d\zeta\, d\square + \boldsymbol{K}_{\Gamma\Gamma}^{geo}, \tag{84}$$

$$\boldsymbol{f}_e^{int} = \int_{\square}\int_{-\frac{h_0}{2}}^{\frac{h_0}{2}} \boldsymbol{B}^T \widehat{\boldsymbol{S}} \sqrt{G}\, d\zeta\, d\square, \tag{85}$$

$$\widetilde{\boldsymbol{f}}_e^{int} = \int_{\square}\int_{-\frac{h_0}{2}}^{\frac{h_0}{2}} \widetilde{\boldsymbol{B}}^T \widehat{\boldsymbol{S}} \sqrt{G}\, d\zeta\, d\square. \tag{86}$$

In (81)–(84), $\mathcal{C}$ is a 6×6 matrix which contains the contravariant components of the fourth order constitutive tensor $\mathcal{C} = 4\nabla^2 W(\boldsymbol{C}) = C^{ijkl}\boldsymbol{G}_i \otimes \boldsymbol{G}_j \otimes \boldsymbol{G}_k \otimes \boldsymbol{G}_l$. The components C^{ijkl} are ordered with respect to the column matrix form (74) of the covariant strain components E_{ij}.

Since the internal degrees of freedom $\boldsymbol{\Gamma}_e$ are only defined on the element level, their increments $\Delta\boldsymbol{\Gamma}_e$ in (80) can be eliminated by static condensation based on the elimination formula

$$\Delta\boldsymbol{\Gamma}_e = -\boldsymbol{K}_{\Gamma\Gamma}^{-1}\left(\widetilde{\boldsymbol{f}}_{int}^e + \boldsymbol{K}_{\Gamma v}\Delta\boldsymbol{v}_e\right). \tag{87}$$

Thus, a generalized displacement problem follows from (80) that is given by

$$\sum_{e=1}^{n_{elem}} \delta\boldsymbol{v}_e \left\{\boldsymbol{r}_e + \boldsymbol{K}_e \Delta\boldsymbol{v}_e\right\} = 0 \tag{88}$$

with the condensed element residual vector and tangent matrix

$$\boldsymbol{r}_e = \boldsymbol{f}_{int}^e - \boldsymbol{f}_{ext}^e - \boldsymbol{K}_{v\Gamma}\boldsymbol{K}_{\Gamma\Gamma}^{-1}\widetilde{\boldsymbol{f}}_{int}^e \qquad \text{and} \qquad \boldsymbol{K}_e = \boldsymbol{K}_{vv} - \boldsymbol{K}_{v\Gamma}\boldsymbol{K}_{\Gamma\Gamma}^{-1}\boldsymbol{K}_{\Gamma v}. \tag{89}$$

After assembly of the element arrays, the corresponding linear algebraic system can be solved for the nodal increments. Then the elimination equation (87) can be used for the update of the internal degrees of freedom, i.e. $\boldsymbol{\Gamma}_e^{(k+1)} = \boldsymbol{\Gamma}_e^{(k)} + \Delta\boldsymbol{\Gamma}_e$, on the element level.

4. Numerical Examples

We present a number of example calculations dealing with thin shell problems as well as large strain applications. The newly developed extensible shell element has been

implemented in an enhanced version of the program FEAP documented in [29]. The aim of our numerical simulations is

- to investigate the significance of the proposed EAS-expansion (23) for the enhanced covariant base vector $\widetilde{\boldsymbol{g}}_3$.
- to show the EAS-improvement of the membrane part by means of the proposed expansion (31) for the enhanced covariant base vectors $\widetilde{\boldsymbol{g}}_\alpha$.
- to verify that the proposed assumed strain interpolation (68) for $\bar{E}_{33}^{\{0\}}$ in conjunction with the simple interpolation (61) of the extensible director field improves the performance in the thin-shell limit considerably and makes the developed shell formulation competitive with more elaborate formulations based on rotational degrees of freedom.
- to verify that three-dimensional constitutive models can be implemented without any shell specific modifications. To this end, compressible and quasi-incompressible hyperelastic materials of the St. Venant-Kirchhoff, Neo-Hookean and Mooney-Rivlin type are particularly used.

The following formulations are employed in the numerical simulations:

A) Newly developed extensible shell formulation based on the proposed EAS-expansions of the enhanced covariant base vectors $\widetilde{\boldsymbol{g}}_i$, equations (23) and (31), in conjunction with the assumed strain interpolation (68) of $\bar{E}_{33}^{\{0\}}$.
B) Bilinear inextensible shell formulation in conjunction with the zero normal stress condition and rotational degrees of freedom as suggested by Simo, Fox & Rifai [4].
C) The same as formulation A, but without the assumed strain interpolation (68) for $\bar{E}_{33}^{\{0\}}$.

4.1. Plane Strain Tension Test

This large strain example illustrates the significant improvement of the membrane part of the proposed shell element by means of the expansion (31) for the enhanced covariant base vectors $\widetilde{\boldsymbol{g}}_\alpha$. As in Miehe [30] we consider an initially square block (see Fig. 2) which is stretched within a displacement controlled calculation. Using the present shell formulation A, the plane strain condition is modeled by constraining the thickness extensibility as a boundary condition. We employ the three-dimensional Neo-Hookean material model with the strain energy function

$$W = \tfrac{\mu}{2}(J^{-\frac{2}{3}} I_1 - 3) + U(J), \qquad U(J) = K(\tfrac{1}{2}(J^2 - 1) - \ln J). \tag{90}$$

Within a penalty formulation, quasi-incompressibility is enforced by the penalty parameter $K = 1.7 \cdot 10^4$ and the material constant $\mu = 33.4$. Due to the symmetry of the problem, only one-quarter of the block has been discretized by $n \times n$ finite element meshes. Fig. 3 depicts the calculated force F for an extension of $u = 40$. The present formulation is compared with the Q1/P0 element described by Simo, Taylor & Pister [31].

We remark further that the pure displacement formulation (obtained in the present formulation by merely dropping the EAS-expansion (31) for $\widetilde{\boldsymbol{g}}_\alpha$) exhibits severe locking in the incompressible limit.

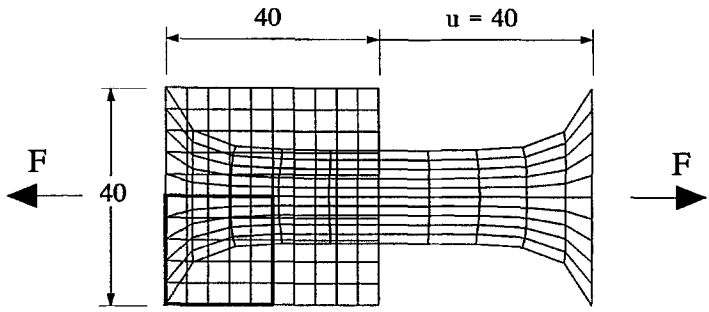

Fig. 2. Plane strain tension test, initial and deformed mesh configuration, 5×5 elements (one-quarter).

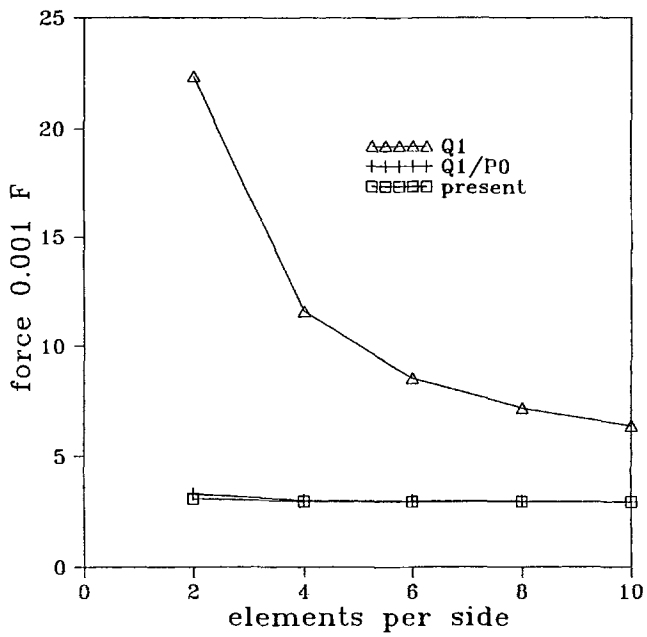

Fig. 3. Plane strain tension test, calculated force for an extension $u = 40$, $n \times n$ elements (one-quarter).

Finally we consider in Fig. 4 an arbitrarily distorted 4×4 mesh (one quarter) of the initial configuration. The corresponding deformed mesh configuration ($u = 40$) of the proposed shell formulation A is plotted with a dash. Even for these irregular element geometries the calculated force deviates from the regular 4×4 mesh less than three per cent.

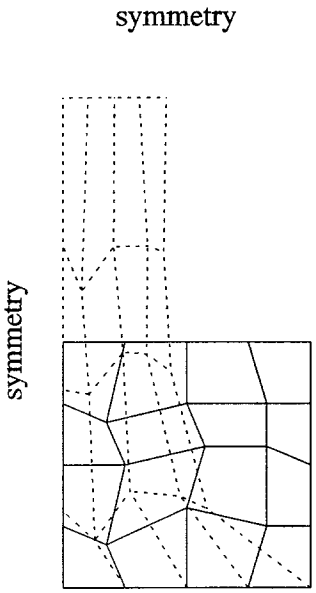

Fig. 4. Plane strain tension test, arbitrarily distorted initial and corresponding deformed 4 × 4 mesh (one-quarter) for an extension $u = 40$.

4.2. Shearing of a Twisted Ribbon

This linear problem shows the significance of the proposed expansions (31) and (23) for the enhanced covariant base vectors $\widetilde{\boldsymbol{g}}_\alpha$ and $\widetilde{\boldsymbol{g}}_3$, respectively. A shell twisted 90°, with length $l = 12$, width $w = 1.1$, thickness $h_0 = 0.32$, and material properties $E = 2.9 \cdot 10^7$, $\nu = 0.22$ is clamped and subjected to a shear load in thickness direction $F = 1$, see Fig. 5. The displacements in load direction are reported for a sequence of finite element meshes in Table 1. They are normalized with respect to the theoretical solution $u = 1.754 \times 10^{-3}$ [32]. The improved performance of the proposed formulation A due to the enhanced covariant base vectors $\widetilde{\boldsymbol{g}}_\alpha$ and $\widetilde{\boldsymbol{g}}_3$ is obvious.

Table 1. Shearing of a twisted ribbon, normalized displacements in load direction.

Mesh	1 × 6	2 × 12	2 × 24	4 × 48
With $\widetilde{g}_3$	0.800	0.917	0.970	0.990
With $\widetilde{g}_3$ and $\widetilde{g}_\alpha$	0.947	0.983	0.993	0.996
Without $\widetilde{g}_i$	0.766	0.881	0.934	0.954

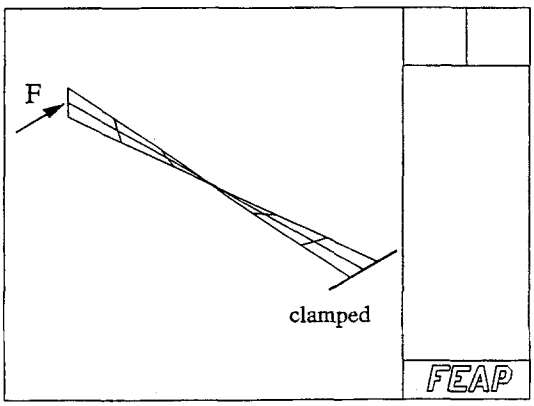

Fig. 5. Shearing of a twisted ribbon. Problem definition and mesh discretization.

4.3. Roll-Up of a Clamped Beam

An initially flat shell of length $L = 10$, width $w = 1$, thickness $h_0 = 0.01$, and material properties $E = 1.2 \times 10^7$, $\nu = 0$ is clamped on one end and subjected to a bending moment on the other end. The exact solution to this problem is a circular curve with radius $R = EI/M$. An applied bending moment of $M = 2\pi EI/L$ forces the beam to roll up into a closed circle.

Since formulations A and C contain no rotational degrees of freedom, the bending moment can not be applied directly. However, as shown in Appendix A.3, a follower load distribution acting along the edge of the current configuration can be accommodated to model this load case.

Figures 6 and 7 depict the initial and final deformed mesh configuration for discretizations with 10 and 20 elements, respectively. Formulation C exhibits severe locking behavior due to parasitic thickness strains. The proposed formulation A yields the same response as the formulation B (which incorporates rotational degrees of freedom) without any artificial thickness change. Thus, the eminent meaning of the proposed assumed strain modification (68) of $\bar{E}_{33}^{\{0\}}$ is obvious.

4.4. Pinched Hemisphere with 18° Hole

A hemispheric shell with an 18° hole at the top is loaded at the free edge with two inward and two outward forces 90° apart. Symmetry conditions are used on this problem and only one quarter of the shell is modeled. The material properties are $E = 6.825 \times 10^7$ and $\nu = 0.3$, the radius is $R = 10$ and the thickness is $h_0 = 0.04$.

The obtained results of the linear calculation are listed in Table 2 for three mesh configurations. There, the values for the displacements under the unit loads are normalized with respect to the solution of 0.093, reported in [33]. It can be seen that the formulation C locks in the case of initial curvature and coarse meshes. On the other hand, formulation

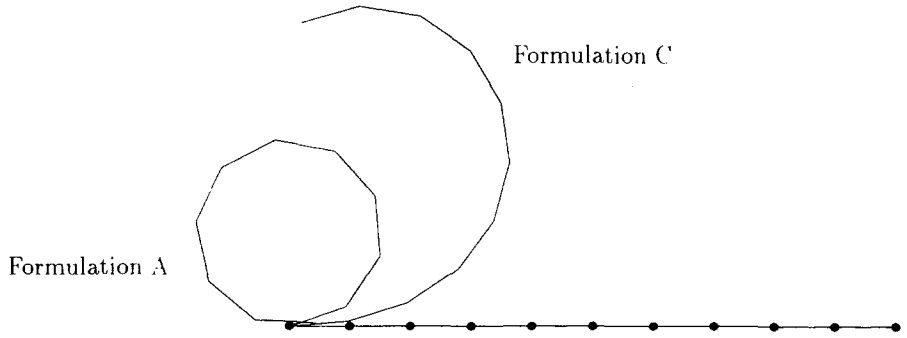

Fig. 6. Roll–up of a clamped beam, 10 elements.

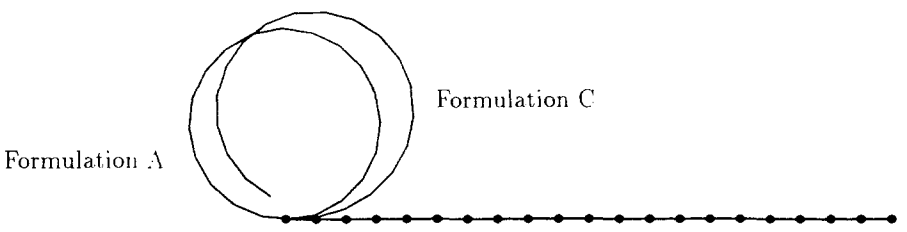

Fig. 7. Roll-up of a clamped beam, 20 elements.

A does not suffer from parasitic transverse normal strains due to the proposed assumed strain modification (68).

For the nonlinear calculation we chose a thickness of $h_0 = 0.01$ in order to yield a radius to thickness ratio of $R/h_0 = 1000$. The same problem has been considered by Simo, Rifai & Fox [7] for the investigation of the thin-shell behavior. A mesh consisting of 16×16 elements has been used to obtain the load-deflection curves plotted in Fig. 8. Formulation C locks progressively with an increasing load due to artificial thickness strains. In contrast to the pathological locking behavior of formulation C, the proposed formulation A yields the same results as the rotational formulation B.

Table 2. Pinched hemisphere, linear solution for the normalized displacements under the load.

Elements	4×4	8×8	16×16
Formulation A	1.026	1.002	0.999
Formulation B	0.985	0.992	0.997
Formulation C	0.083	0.845	0.995

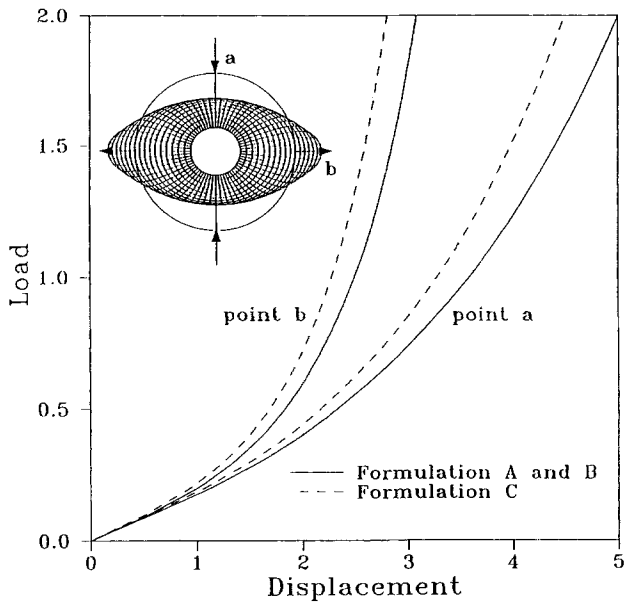

Fig. 8. Pinched hemisphere, $h_0/R = 1 \cdot 10^{-3}$, load-deflection curves of the nonlinear calculation, 16 × 16 elements.

4.5. Bending and Inflation of a Circular Plate

This large strain problem has been previously investigated by Hughes & Carnoy [34] and Parisch [35]. A circular plate with radius $r = 7.5$ and thickness $h_0 = 0.5$ is simply supported at the circumference and subjected to uniform pressure acting perpendicular to the current configuration. The deformation dependent pressure p leads to an additional (nonsymmetric) contribution to the tangential stiffness matrix $(81)_1$, see e.g. Schweizerhof & Ramm [36]. Because of the symmetry of the problem, only one quarter of the plate has been discretized.

Infinitesimal theory. First, we demonstrate the significance of the proposed EAS-expansion (23) for the enhanced covariant base vector $\widetilde{g}_3$ of formulation A by means of the linear calculations. The material parameters of the three-dimensional St. Venant-Kirchoff model are $E = 600$ and $\nu = 0.4999$ so that a quasi-incompressible response is enforced. For $p = 0.01$ and a discretization with 108 elements, the plane stress formulation B yields a deflection $w_R = 0.2190$ of the plate center. Table 3 reports the normalized results w/w_R for different meshes. There, nt denotes the employed number of internal degrees of freedom for $\widetilde{g}_3$ in (23). The significance of the proposed EAS-expansion in the bending dominated case is evident.

Table 3. Bending and inflation of a circular plate, normalized deflection w/w_R of the plate center of the linear calculations. *nt*: number of internal degrees of freedom.

Number of elements		3	12	27	48	108
Inextensible theory, plane stress		0.915	0.986	0.995	0.998	1.000
Extensible theory	$nt = 4$	0.913	0.984	0.994	0.997	0.999
Formulation A	$nt = 1$	0.673	0.784	0.818	0.839	0.873
	$nt = 0$	0.006	0.007	0.007	0.007	0.007

Nonlinear theory. In the nonlinear regime the plate is made of an incompressible hyperelastic material described by the Mooney-Rivlin model with strain energy function

$$W = c_1(I_1 - 3) + c_2(I_2 - 3) + U(J),$$
$$U(J) = \frac{\lambda}{2}(\ln J)^2 - 2(c_1 + 2c_2)\ln J. \tag{91}$$

In (91), $U(J)$ denotes the extension to the compressible range of the constitutive model for the incompressible material. The material constants are $c_1 = 80$ and $c_2 = 20$. We enforce the incompressibility constraint by means of a penalty-parameter $\lambda = 50000$. In Fig. 9 the applied value of the pressure is plotted versus the deflection of the plate center. The computed results of the proposed formulation A, obtained with three Gauss integration points through the thickness and $nt = 4$, are compared to calculations using the membrane element presented by Gruttmann & Taylor [37] and to the shell element of Parisch [35], respectively. Both formulations satisfy incompressibility in an exact manner using the plane stress condition. It can be seen that the results fit very well. Fig. 10 depicts a sequence of deformed configurations for increasing pressure loads.

5. Conclusions

A nonlinear continuum-based 4-node shell element is presented which relies on extensible director kinematics. Within the proposed curvilinear representation of the nonlinear EAS method of Simo & Armero [1], it is shown that the local expansion of the enhanced material displacement gradient leads to enhanced covariant base vectors which are superposed on the compatible covariant base vectors. Two expansions of the enhanced covariant base vectors are developed: First, the underlying extensible shell kinematic is extended and, as a consequence, full three-dimensional constitutive models can be implemented without resorting to the plane stress assumption. Second, the membrane part of the bilinear compatible finite element interpolation is improved. Furthermore, parasitic strain effects of the compatible interpolation are eliminated by means of two assumed strain modifications.

Numerical examples confirm that the element performance is competitive with more elaborate formulations which require an orthogonal matrix in order to describe finite rotations, even in the case of very thin shells. Furthermore, it is shown that the developed extensible shell element is able to deal with large strain problems.

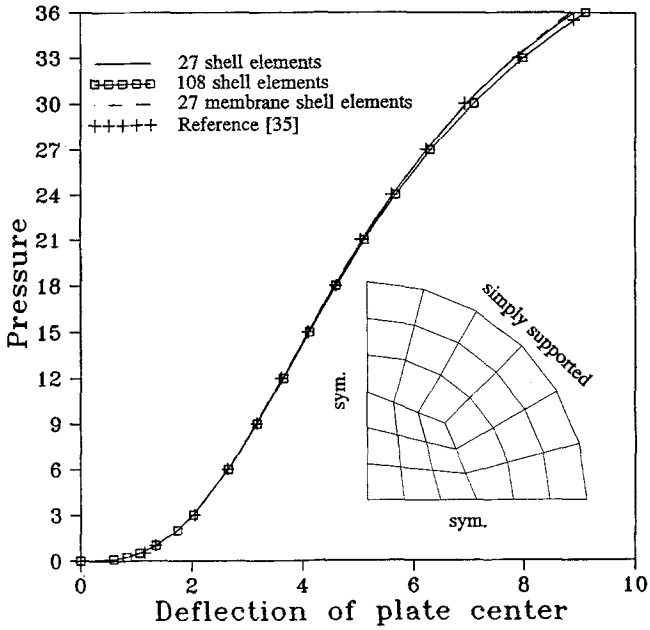

Fig. 9. Bending and inflation of a circular plate. Discretized quarter of the plate (27 elements) and plot of pressure versus deflection at plate center.

Appendix A

A.1. Discrete Operator Matrices

In this section we derive the submatrices of the discrete operator matrices $\boldsymbol{B}_I$ and $\widetilde{\boldsymbol{B}}$ in (77).

Contribution of the tangential strains. Using (42), i.e. $\psi = \varphi_{,\alpha} + \widetilde{\varphi}_\alpha$, together with the EAS-expansion (31) for $\widetilde{\varphi}_\alpha$ leads to

$$\psi_\alpha = \varphi_{,\alpha} + \sum_{J=1}^{2} a_\alpha^J \Gamma_J^\beta \varphi_{0,\beta} \tag{92}$$

$$\psi_\alpha = \sum_{I=1}^{4} M_\alpha^I \varphi_I \qquad \text{with} \qquad M_\alpha^I = N_{,\alpha}^I + \sum_{J=1}^{2} a_\alpha^J \Gamma_J^\beta N_{0,\beta}^I, \tag{93}$$

where the compatible interpolation (60) of the mid-surface has been introduced. Next, the discrete form of the linearized covariant base vectors (41), i.e. $\delta \boldsymbol{g}_\alpha = \delta\psi_\alpha + \zeta \delta \boldsymbol{d}_{,\alpha}$, yields

$$\delta \boldsymbol{g}_\alpha = \sum_{I=1}^{4} [M_\alpha^I \delta\varphi_I + \zeta N_{,\alpha}^I \delta \boldsymbol{d}_I] + \sum_{J=1}^{2} a_\alpha^J \varphi_{0,\gamma} \delta\Gamma_J^\gamma. \tag{94}$$

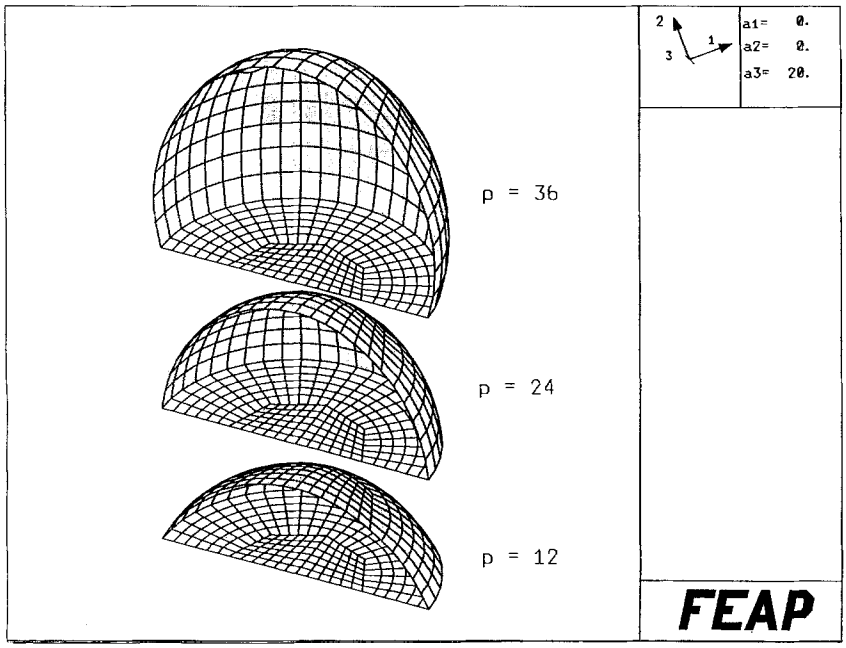

Fig. 10. Bending and inflation of a circular plate. Sequence of deformed configurations (mesh consists of 108 elements per quarter).

Therefore, the variation of the discrete tangential strains can be calculated via

$$\delta E_{\alpha\beta} = \frac{1}{2}\left[\delta \boldsymbol{g}_\alpha \cdot \boldsymbol{g}_\beta + \boldsymbol{g}_\alpha \cdot \delta \boldsymbol{g}_\beta\right] \tag{95}$$

so that one obtains

$$\begin{bmatrix} \delta E_{11} \\ \delta E_{22} \\ 2\delta E_{12} \end{bmatrix} = \sum_{I=1}^{4} [\boldsymbol{B}_I^{\varphi} \delta \boldsymbol{\varphi}_I + \boldsymbol{B}_I^{d} \delta \boldsymbol{d}_I] + \sum_{J=1}^{2} \widetilde{\boldsymbol{B}}_J^{m} \delta \boldsymbol{\Gamma}_J, \tag{96}$$

where

$$\boldsymbol{B}_I^{\varphi} = \begin{bmatrix} M_1^I \boldsymbol{g}_1^T \\ M_2^I \boldsymbol{g}_2^T \\ M_1^I \boldsymbol{g}_2^T + M_2^I \boldsymbol{g}_1^T \end{bmatrix} \quad \text{and} \quad \boldsymbol{B}_I^{d} = \zeta \begin{bmatrix} N_1^I \boldsymbol{g}_1^T \\ N_2^I \boldsymbol{g}_2^T \\ N_1^I \boldsymbol{g}_2^T + N_2^I \boldsymbol{g}_1^T \end{bmatrix} \tag{97}$$

and

$$\widetilde{\boldsymbol{B}}_J^{m} = \begin{bmatrix} a_1^J b_{11} & a_1^J b_{21} \\ a_2^J b_{12} & a_2^J b_{22} \\ a_1^J b_{12} + a_2^J b_{11} & a_1^J b_{22} + a_2^J b_{21} \end{bmatrix} \quad \text{with} \quad b_{\alpha\beta} = \boldsymbol{\varphi}_{0,\alpha} \cdot \boldsymbol{g}_\beta. \tag{98}$$

Contribution of the thickness strains. The variation of the discrete thickness strains is given by

$$\delta E_{33} = \delta \bar{E}_{33}^{\{0\}} + \zeta \delta E_{33}^{\{1\}}, \tag{99}$$

where the first term has been derived in (70) from the proposed assumed strain interpolation (68) so that

$$\delta \bar{E}_{33}^{\{0\}} = \sum_{I=1}^{4} N^I \boldsymbol{d}_I^T \delta \boldsymbol{d}_I. \tag{100}$$

The second term in (99) follows from the proposed EAS-extension in section 3.2 and can be written in the form

$$\delta E_{33}^{\{1\}} = 2\tilde{\gamma} \boldsymbol{d} \cdot \delta \boldsymbol{d} + \|\boldsymbol{d}\|^2 \delta \tilde{\gamma} \tag{101}$$

$$\delta E_{33}^{\{1\}} = \sum_{I=1}^{4} [2\tilde{\gamma} N^I \boldsymbol{d}^T] \boldsymbol{d}_I + \|\boldsymbol{d}\|^2 \boldsymbol{e}^T \delta \boldsymbol{\Gamma}_d. \tag{102}$$

As a result we obtain

$$\delta E_{33} = \sum_{I=1}^{4} \boldsymbol{b}_I^{33} \delta \boldsymbol{d}_I + \tilde{\boldsymbol{b}}^{33} \delta \boldsymbol{\Gamma}_d \tag{103}$$

with

$$\boldsymbol{b}_I^{33} = N^I \boldsymbol{d}_I^T + 2\zeta \tilde{\gamma} N^I \boldsymbol{d}^T \qquad \text{and} \qquad \tilde{\boldsymbol{b}}^{33} = \zeta \|\boldsymbol{d}\|^2 \boldsymbol{e}^T. \tag{104}$$

Contribution of the transverse shear strains. Following Dvorkin & Bathe [17], the assumed strain interpolation of the constant transverse shear strains $\bar{E}_{\alpha 3}^{\{0\}}$ is based on the compatible transverse shear strains $E_{\alpha 3}^{\{0\}}$ collocated at the midpoints $Q = A, B, C, D$ of the element boundaries:

$$\begin{bmatrix} 2\bar{E}_{13}^{\{0\}} \\ 2\bar{E}_{23}^{\{0\}} \end{bmatrix} = \begin{bmatrix} (1-\xi^2) E_{13B}^{\{0\}} + (1+\xi^2) E_{13D}^{\{0\}} \\ (1-\xi^1) E_{23A}^{\{0\}} + (1+\xi^1) E_{23C}^{\{0\}} \end{bmatrix}, \tag{105}$$

where the compatible covariant transverse shear strains are given by

$$E_{\alpha 3}^{\{0\}} = \frac{1}{2} [\boldsymbol{\varphi}_{,\alpha} \cdot \boldsymbol{d} - \boldsymbol{\Phi}_{,\alpha} \cdot \boldsymbol{D}]. \tag{106}$$

The total transverse shear strains can be written in the form

$$E_{\alpha 3} = \bar{E}_{\alpha 3}^{\{0\}} + \zeta E_{\alpha 3}^{\{1\}} \qquad \text{with} \qquad E_{\alpha 3}^{\{1\}} = \frac{1}{2} [\boldsymbol{d} \cdot \boldsymbol{d}_{,\alpha} - \boldsymbol{D} \cdot \boldsymbol{D}_{,\alpha}]. \tag{107}$$

Variation of (107) yields

$$\begin{bmatrix} 2\delta E_{13} \\ 2\delta E_{23} \end{bmatrix} = \bar{\boldsymbol{B}}_{\varphi}^{S} \delta \boldsymbol{\varphi}_e + \boldsymbol{B}_d^S \delta \boldsymbol{d}_e, \tag{108}$$

with

$$\bar{\boldsymbol{B}}^S_{\varphi} = \frac{1}{4}\begin{bmatrix} -(1-\xi^2)\boldsymbol{d}_B^T & (1-\xi^2)\boldsymbol{d}_B^T & (1+\xi^2)\boldsymbol{d}_D^T & -(1+\xi^2)\boldsymbol{d}_D^T \\ -(1-\xi^1)\boldsymbol{d}_A^T & -(1+\xi^1)\boldsymbol{d}_C^T & (1+\xi^1)\boldsymbol{d}_C^T & (1-\xi^1)\boldsymbol{d}_A^T \end{bmatrix},$$

$$\boldsymbol{B}^S_d = \bar{\boldsymbol{B}}^S_d + \zeta \boldsymbol{B}^{\{1\}}_{(\alpha 3)}$$

$$\bar{\boldsymbol{B}}^S_d = \frac{1}{4}\begin{bmatrix} (1-\xi^2)\boldsymbol{\varphi}_{,1}^{B^T} & (1-\xi^2)\boldsymbol{\varphi}_{,1}^{B^T} & (1+\xi^2)\boldsymbol{\varphi}_{,1}^{D^T} & (1+\xi^2)\boldsymbol{\varphi}_{,1}^{D^T} \\ (1-\xi^1)\boldsymbol{\varphi}_{,2}^{A^T} & (1+\xi^1)\boldsymbol{\varphi}_{,2}^{C^T} & (1+\xi^1)\boldsymbol{\varphi}_{,2}^{C^T} & (1-\xi^1)\boldsymbol{\varphi}_{,2}^{A^T} \end{bmatrix},$$

$$\boldsymbol{B}^{\{1\}}_{(\alpha 3)I} = \begin{bmatrix} N^I \boldsymbol{d}_{,1}^T + N^I_{,1}\boldsymbol{d}^T \\ N^I \boldsymbol{d}_{,2}^T + N^I_{,2}\boldsymbol{d}^T \end{bmatrix}.$$

A.2. The Geometric Part of the Tangent Matrix

In this section we derive the geometric part of the tangent submatrices in (81)–(84). The contribution of the nodes I and K to the tangent submatrix $\boldsymbol{K}_{vv}$ in (81) can be written in the form

$$(\boldsymbol{K}^{geo}_{vv})_{IK} = \begin{bmatrix} \boldsymbol{K}^{geo}_{\varphi\varphi} & \boldsymbol{K}^{geo}_{\varphi d} \\ \boldsymbol{K}^{geo}_{d\varphi} & \boldsymbol{K}^{geo}_{dd} \end{bmatrix}_{IK} \tag{109}$$

with

$$(\boldsymbol{K}^{geo}_{\varphi\varphi})_{IK} = (\boldsymbol{K}^{\alpha\beta}_{\varphi\varphi})_{IK}, \tag{110}$$

$$(\boldsymbol{K}^{geo}_{\varphi d})_{IK} = (\boldsymbol{K}^{\alpha\beta}_{\varphi d})_{IK} + (\boldsymbol{K}^{\alpha 3}_{\varphi d})_{IK}, \tag{111}$$

$$(\boldsymbol{K}^{geo}_{d\varphi})_{IK} = (\boldsymbol{K}^{\alpha\beta}_{d\varphi})_{IK} + (\boldsymbol{K}^{\alpha 3}_{d\varphi})_{IK}, \tag{112}$$

$$(\boldsymbol{K}^{geo}_{dd})_{IK} = (\boldsymbol{K}^{\alpha\beta}_{dd})_{IK} + (\boldsymbol{K}^{33}_{dd})_{IK} + (\boldsymbol{K}^{\alpha 3}_{dd})_{IK}, \tag{113}$$

where the superscript $\alpha\beta$ denotes the contribution of the tangential strains. Corresponding to this, the superscripts $\alpha 3$ and 33 denote the contribution of the transverse shear strains and the transverse normal strains, respectively.

Analogously, the tangent submatrix $\boldsymbol{K}_{v\Gamma}$ in (82) is given by

$$(\boldsymbol{K}^{geo}_{v\Gamma})_I = \begin{bmatrix} \boldsymbol{K}^{geo}_{\varphi\Gamma} \\ \boldsymbol{K}^{geo}_{d\Gamma} \end{bmatrix}_I = \begin{bmatrix} \boldsymbol{0}_{3\times nt} & \boldsymbol{K}^{\alpha\beta}_{\varphi\Gamma_1} & \boldsymbol{K}^{\alpha\beta}_{\varphi\Gamma_2} \\ \boldsymbol{K}^{33}_{d\Gamma_d} & \boldsymbol{K}^{\alpha\beta}_{d\Gamma_1} & \boldsymbol{K}^{\alpha\beta}_{d\Gamma_2} \end{bmatrix}_I, \tag{114}$$

and the tangent submatrix $\boldsymbol{K}_{\Gamma\Gamma}$ in (84) can be written in the form

$$\boldsymbol{K}^{geo}_{\Gamma\Gamma} = \begin{bmatrix} \boldsymbol{0}_{nt\times nt} & \boldsymbol{0}_{nt\times 2} & \boldsymbol{0}_{nt\times 2} \\ \boldsymbol{0}_{2\times nt} & \boldsymbol{K}^{\alpha\beta}_{\Gamma_1\Gamma_1} & \boldsymbol{K}^{\alpha\beta}_{\Gamma_1\Gamma_2} \\ \boldsymbol{0}_{2\times nt} & \boldsymbol{K}^{\alpha\beta}_{\Gamma_2\Gamma_1} & \boldsymbol{K}^{\alpha\beta}_{\Gamma_2\Gamma_2} \end{bmatrix}. \tag{115}$$

Next, we derive the submatrices in (110)–(115).

Contribution of the tangential strains. The contribution of the tangential strains to the geometric part of the tangent matrix is given by

$$\int\!\!\int_{\square}\int_{-\frac{h_0}{2}}^{\frac{h_0}{2}} \Delta\{\delta \boldsymbol{g}_\alpha \cdot \boldsymbol{g}_\beta\}\hat{S}^{\alpha\beta}\sqrt{G}\,d\zeta\,d\square$$

$$= \int\!\!\int_{\square}\int_{-\frac{h_0}{2}}^{\frac{h_0}{2}} \{\delta \boldsymbol{g}_\alpha \cdot \Delta\boldsymbol{g}_\beta + \Delta\delta \boldsymbol{g}_\alpha \cdot \boldsymbol{g}_\beta\}\hat{S}^{\alpha\beta}\sqrt{G}\,d\zeta\,d\square.$$

The second variation of the discrete covariant base vectors (94) is given by

$$\Delta\delta \boldsymbol{g}_\alpha = \sum_{I=1}^{4}\sum_{J=1}^{2} \delta\varphi_I N^I_{0,\gamma} a^J_\alpha \Delta\Gamma^\gamma_J + \sum_{M=1}^{2}\sum_{K=1}^{4} \delta\Gamma^\gamma_M a^M_\alpha N^K_{0,\gamma}\Delta\varphi_K. \tag{116}$$

Thus, we obtain the following contributions to the equations (110–113), (114) and (115):

$$(\boldsymbol{K}^{\alpha\beta}_{\upsilon\upsilon})_{IK} = \int\!\!\int_{\square}\int_{-\frac{h_0}{2}}^{\frac{h_0}{2}} \begin{bmatrix} M^I_\alpha M^K_\beta \hat{S}^{\alpha\beta}\mathbf{1}_{3\times3} & \zeta M^I_\alpha N^K_{,\beta}\hat{S}^{\alpha\beta}\mathbf{1}_{3\times3} \\ \zeta N^I_{,\alpha} M^K_\beta \hat{S}^{\alpha\beta}\mathbf{1}_{3\times3} & \zeta^2 N^I_{,\alpha} N^K_{,\beta}\hat{S}^{\alpha\beta}\mathbf{1}_{3\times3} \end{bmatrix}\sqrt{G}\,d\zeta\,d\square,$$

$$(\boldsymbol{K}^{\alpha\beta}_{\varphi\Gamma_J})_I = \int\!\!\int_{\square}\int_{-\frac{h_0}{2}}^{\frac{h_0}{2}} (M^I_\alpha a^J_\beta \hat{S}^{\alpha\beta})\sqrt{G}\,d\zeta\,d\square \begin{bmatrix} \varphi_{0.1} & \varphi_{0.2} \end{bmatrix}$$

$$+ \int\!\!\int_{\square}\int_{-\frac{h_0}{2}}^{\frac{h_0}{2}} \begin{bmatrix} (a^J_\alpha \boldsymbol{g}_\beta \hat{S}^{\alpha\beta})N^I_{0.1} & (a^J_\alpha \boldsymbol{g}_\beta \hat{S}^{\alpha\beta})N^I_{0.2} \end{bmatrix}\sqrt{G}\,d\zeta\,d\square,$$

$$(\boldsymbol{K}^{\alpha\beta}_{d\Gamma_J})_I = \int\!\!\int_{\square}\int_{-\frac{h_0}{2}}^{\frac{h_0}{2}} \zeta(N^I_{,\alpha} a^J_\beta \hat{S}^{\alpha\beta})\sqrt{G}\,d\zeta\,d\square \begin{bmatrix} \varphi_{0.1} & \varphi_{0.2} \end{bmatrix},$$

$$\boldsymbol{K}^{\alpha\beta}_{\Gamma_J\Gamma_M} = \int\!\!\int_{\square}\int_{-\frac{h_0}{2}}^{\frac{h_0}{2}} (a^J_\alpha a^M_\beta \hat{S}^{\alpha\beta})\sqrt{G}\,d\zeta\,d\square \begin{bmatrix} \varphi_{0.1}\cdot\varphi_{0.1} & \varphi_{0.1}\cdot\varphi_{0.2} \\ \varphi_{0.2}\cdot\varphi_{0.1} & \varphi_{0.2}\cdot\varphi_{0.2} \end{bmatrix}.$$

Contribution of the thickness strains. The contribution of the thickness strains to the geometric part of the tangent matrix is given by

$$\int\!\!\int_{\square}\int_{-\frac{h_0}{2}}^{\frac{h_0}{2}} \Delta\delta E_{33}\hat{S}^{33}\sqrt{G}\,d\zeta\,d\square. \tag{117}$$

From (103) we obtain the following contributions to (113) and (114):

$$(\boldsymbol{K}^{33}_{dd})_{IK} = \int\!\!\int_{\square}\int_{-\frac{h_0}{2}}^{\frac{h_0}{2}} N^I(\delta^K_I + 2\zeta\tilde{\gamma}N^K)\hat{S}^{33}\sqrt{G}\,d\zeta\,d\square\mathbf{1}_{3\times3},$$

$$(\boldsymbol{K}^{33}_{d\Gamma_d})_I = \int\!\!\int_{\square}\int_{-\frac{h_0}{2}}^{\frac{h_0}{2}} (2\zeta N^I \hat{S}^{33}\boldsymbol{d}\otimes\boldsymbol{e})\sqrt{G}\,d\zeta\,d\square.$$

Contribution of the Transverse Shear Strains. The contribution of the transverse shear strains to the geometric part of the tangent matrix is given by

$$\int\!\!\int_{\square} \int_{-\frac{h_0}{2}}^{\frac{h_0}{2}} \Delta\delta E_{\alpha 3} \hat{S}^{\alpha 3} \sqrt{G}\, d\zeta\, d\square. \tag{118}$$

From (108) we obtain the following contributions to the equations (111–113):

$$\boldsymbol{K}^{\alpha 3}_{\varphi d} = \int\!\!\int_{\square} \int_{-\frac{h_0}{2}}^{\frac{h_0}{2}} \begin{bmatrix} -(A+B)\mathbf{1} & -B\mathbf{1} & \mathbf{0} & -A\mathbf{1} \\ B\mathbf{1} & (B-C)\mathbf{1} & -C\mathbf{1} & \mathbf{0} \\ \mathbf{0} & C\mathbf{1} & (C+D)\mathbf{1} & D\mathbf{1} \\ A\mathbf{1} & \mathbf{0} & -D\mathbf{1} & (A-D)\mathbf{1} \end{bmatrix} \sqrt{G}\, d\zeta\, d\square,$$

$$A = \tfrac{1}{4}(1-\xi^1)\hat{S}^{23} \quad B = \tfrac{1}{4}(1-\xi^2)\hat{S}^{13} \quad C = \tfrac{1}{4}(1+\xi^1)\hat{S}^{23} \quad D = \tfrac{1}{4}(1+\xi^2)\hat{S}^{13},$$

$$\boldsymbol{K}^{\alpha 3}_{d\varphi} = \boldsymbol{K}^{\alpha 3^T}_{\varphi d},$$

$$(\boldsymbol{K}^{\alpha 3}_{dd})_{IK} = \int\!\!\int_{\square} \int_{-\frac{h_0}{2}}^{\frac{h_0}{2}} \zeta [N^I N^K_{,\alpha} + N^I_{,\alpha} N^K] \hat{S}^{\alpha 3} \sqrt{G}\, d\zeta\, d\square \mathbf{1}_{3\times 3}.$$

A.3. Load Case Bending Moment

The numerical example 4.3 'roll-up of a clamped beam' requires the application of a bending moment at the end of the beam. Since formulations A and C do not incorporate any rotational degrees of freedom, we subject the shell to follower end loads to model this load case. In this Appendix $\boldsymbol{g}_i$ and $\boldsymbol{g}^i$ denote the compatible covariant and contravariant base vectors, respectively. We consider a stress distribution, linear over the shell thickness, acting along the edge $\xi^1 = \text{constant}$ of the current configuration. Accordingly, the first Piola-Kirchhoff stress tensor

$$\boldsymbol{P} = \frac{M}{I}\zeta \frac{\boldsymbol{g}^1}{\|\boldsymbol{g}^1\|} \otimes \boldsymbol{N} \qquad \text{with} \qquad \boldsymbol{g}^1 = \frac{1}{\sqrt{g}} \boldsymbol{g}_2 \times \boldsymbol{d} \qquad \text{and} \qquad I = \frac{w\, h_0^3}{12} \tag{119}$$

leads to the external loading contribution to the weak form

$$G_{ext} = \int_{\partial \mathcal{B}_{0t}} \delta \boldsymbol{x} \cdot \boldsymbol{P} \boldsymbol{N}\, dA. \tag{120}$$

For the present example, the center-line of the initial configuration coincides with the $x-$ axis, i.e. $\boldsymbol{N} = \boldsymbol{e}_1$, and the axis of rotation coincides with the $y-$ axis, i.e. $\boldsymbol{g}_2/\|\boldsymbol{g}_2\| = \boldsymbol{e}_2$. Therefore

$$\frac{\boldsymbol{g}^1}{\|\boldsymbol{g}^1\|} = \boldsymbol{e}_2 \times \frac{\boldsymbol{d}}{\|\boldsymbol{d}\|} \qquad \text{and} \qquad dA = dy\, d\zeta. \tag{121}$$

Applying shell kinematics leads to the contribution to the weak form of momentum balance

$$G_{ext} = \delta \boldsymbol{d}^T M \left(\boldsymbol{e}_2 \times \frac{\boldsymbol{d}}{\|\boldsymbol{d}\|} \right). \tag{122}$$

The linearization of equation (122) has to be taken into account in order to reach asymptotically quadratic rates of convergence for the Newton iteration solution procedure. One obtains the contribution to the tangent stiffness matrix

$$DG_{ext} \cdot \Delta \boldsymbol{d} = \delta \boldsymbol{d}^T M \frac{1}{\|\boldsymbol{d}\|} \left(\widehat{\boldsymbol{e}}_2 + \left[\frac{\boldsymbol{d}}{\|\boldsymbol{d}\|} \times \boldsymbol{e}_2 \right] \otimes \frac{\boldsymbol{d}}{\|\boldsymbol{d}\|} \right) \Delta \boldsymbol{d}, \tag{123}$$

where $\widehat{\boldsymbol{e}}_2$ denotes the skew–symmetric matrix associated with the axial vector $\boldsymbol{e}_2$, defined by the relation $\widehat{\boldsymbol{e}}_2 \boldsymbol{a} = \boldsymbol{e}_2 \times \boldsymbol{a}$ for any $\boldsymbol{a} \in \mathbb{R}^3$.

References

[1] J. C. Simo and F. Armero, Geometrically nonlinear enhanced strain mixed methods and the method of incompatible modes, *Int. J. Num. Meth. Eng.* **33** (1992) 1413–1449.

[2] E. Ramm, Geometrisch nichtlineare Elastostatik und finite Elemente, Habilitation, Bericht Nr. 76-2, Institut für Baustatik, Universität Stuttgart, (1976).

[3] T. J. R. Hughes and W. K. Liu, Nonlinear finite element analysis of shells: Part I. Three–dimensional shells, *Comp. Meth. Appl. Mech. Eng.* **26** (1981) 331–362.

[4] J. C. Simo, D. D. Fox and M. S. Rifai, On a stress resultant geometrically exact shell model. Part III: Computational aspects of the nonlinear theory, *Comp. Meth. Appl. Mech. Eng.* **79** (1990) 21–70.

[5] F. Gruttmann, W. Wagner, P. Wriggers, A nonlinear quadrilateral shell element with drilling degrees of freedom, *Archive Appl. Mech.* **62** (1992) 474–486.

[6] Y. Basar, Y. Ding and W. B. Krätzig, Finite-rotatation shell elements via mixed formulation, *Comp. Mech.* **10** (1992) 289–306.

[7] J. C. Simo, M. S. Rifai and D. D. Fox, On a stress resultant geometrically exact shell model. Part IV: Variable thickness shells with through-the-thickness stretching, *Comp. Meth. Appl. Mech. Eng.* **81** (1990) 91–126.

[8] N. Büchter and E. Ramm, 3d–extension of nonlinear shell equations based on the enhanced assumed strain concept, *Comp. Meth. Appl. Sci.* (1992) 55–62.

[9] N. Büchter, E. Ramm and D. Roehl, Three-dimensional extension of nonlinear shell formulations based on the enhanced assumed strain concept, *Int. J. Num. Meth. Eng.* **37** (1994) 2551–2568.

[10] P. Steinmann, P. Betsch and E. Stein, FE plane stress analysis incorporating arbitrary 3d large strain constitutive models, submitted to *Eng. Comp.* (1994).

[11] P. Betsch, F. Gruttmann and E. Stein, A 4–node finite shell element for the implementation of general hyperelastic 3D–elasticity at finite strains, to appear in *Comp. Meth. Appl. Mech. Eng.* (1994).

[12] C. Sansour, A theory and finite element formulation of shells at finite deformations including thickness change: Circumventing the use of a rotation tensor, *Arch. Appl. Mech.* **65** (1995) 194–216.

[13] A. Kühhorn and H. Schoop, A nonlinear theory for sandwich shells including the wrinkling phenomenon, *Arch. Appl. Mech.* **62** (1992) 413–427.

[14] H. Parisch, A continuum-based shell theory for non-linear applications, *Int. J. Num. Meth. Eng.* **38** (1995) 1855–1883.

[15] H. Schoop, A simple nonlinear flat element for large displacement structures, *Computers & Structures* **32** (1989) 379–385.

[16] J. C. Simo and M. S. Rifai, A class of mixed assumed strain methods and the method of incompatible modes, *Int. J. Num. Meth. Eng.* **29** (1990) 1595–1638.

[17] E. N. Dvorkin and K.-J. Bathe, A continuum mechanics based four-node shell element for general nonlinear analysis, *Eng. Comput.* **1** (1984) 77–88.

[18] K. J. Bathe and E. N. Dvorkin, A four-node plate bending element based on Mindlin/Reissner plate theory and a mixed interpolation, *Int. J. Num. Meth. Eng.* **21** (1985) 367–383.

[19] N. Stander, A. Matzenmiller and E. Ramm, An assessment of assumed strain methods in finite rotation shell analysis, *Eng. Comput.* **6** (1989) 58–66.
[20] H. Parisch, An investigation of a finite rotation four-node assumed strain shell element, *Int. J. Num. Meth. Eng.* **31** (1991) 127–150.
[21] P. Betsch and E. Stein, An assumed strain approach avoiding artificial thickness straining for a nonlinear 4-node shell element, *Comm. Num. Meth. Eng.* **11** (1995) 899–909.
[22] J. C. Simo and T. J. R. Hughes, On the variational foundations of assumed strain methods, *J. Appl. Mech.* **53** (1986) 51–54.
[23] B. D. Reddy and J. C. Simo, Stability and convergence of a class of enhanced strain methods, preprint (1994).
[24] P. M. Naghdi, The theory of plates and shells, in *Handbuch der Physik*, Band VIa/2 (Springer, Berlin, 1972) 425–640.
[25] E. L. Wilson, R. L. Taylor, W. P. Doherty and J. Ghaboussi, Incompatible Displacement Models, Numerical and Computer Models in Structural Mechanics, eds. S. J. Fenves, N. Perrone, A. R. Robinson and W. C. Schnobrich. New York: Academic Press (1973) 43–57.
[26] J. C. Simo, F. Armero and R. L. Taylor, Improved versions of assumed enhanced strain tri-linear elements for 3D finite deformation problems, *Comp. Meth. Appl. Mech. Eng.* **110** (1993) 359–386.
[27] A. E. Green and W. Zerna, *Theoretical Elasticity* (Oxford University Press, London, 1954).
[28] T. J. R. Hughes, *The Finite Element Method* (Prentice Hall, Englewood Cliffs, NJ, 1987).
[29] O. C. Zienkiewicz and R. L. Taylor, *The Finite Element Method, Volume* 1, *Basic Formulation and Linear Problems* (McGraw-Hill, London, 1989).
[30] C. Miehe, Aspects of the formulation and finite element implementation of large strain isotropic elasticity, *Int. J. Num. Meth. Eng.* **37** (1994) 1981–2004.
[31] J. C. Simo, R. L. Taylor and K. S. Pister, Variational and projection methods for the volume constraint in finite deformation elasto-plasticity, *Comp. Meth. Appl. Mech. Eng.* **51** (1985) 177–208.
[32] R. H. MacNeal and R. L. Harder, A proposed standard set of problems to test finite element accuracy, *Finite Elements in Analysis and Design* **1** (1985) 3–20.
[33] J. C. Simo, D. D. Fox and M. S. Rifai, On a stress resultant geometrically exact shell model. Part II: The linear theory; Computational aspects, *Comp. Meth. Appl. Mech. Eng.* **73** (1989) 53–92
[34] T. J. R. Hughes and E. Carnoy, Nonlinear finite element shell formulation accounting for large membrane strains, *Comp. Meth. Appl. Mech. Eng.* **39** (1983) 69–82.
[35] H. Parisch, Efficient non-linear finite element shell formulation involving large strains, *Eng. Comput.* **3** (1986) 121–128.
[36] K. Schweizerhof and E. Ramm, Displacement dependent pressure loads in nonlinear finite element analyses, *Comput. Struct.* **18** (1984) 1099–1114.
[37] F. Gruttmann and R. L. Taylor, Theory and finite element formulation of rubberlike membrane shells using principal stretches, *Int. J. Num. Meth. Eng.* **35** (1992) 1111–1126.